1971

Charge storage on emulsion and photoresist irradiated by an electron beam

Arthur K. Kreider
Lehigh University

CHARGE STORAGE ON EMULSION AND PHOTORESIST IRRADIATED BY AN ELECTRON BEAM

by
Arthur K. Kreider

ABSTRACT

Surface potentials have been measured on photosensitive materials after irradiation by an electron beam. Kodak HRP emulsion was irradiated with 6.2×10^{-9} coul/cm^2 and an order of magnitude above and below this value. Kodak KTFR was similarly irradiated at, above and below 6.2×10^{-6} coul/cm^2. Both materials were irradiated with 5, 10 and 15 KV electrons.

The resulting potentials were measured with a Kelvin Probe device featuring synchronous detection, phase adjustment and continuous data output.

The photosensitive materials were evaluated on glass substrates, with and without metal cladding on the glass. When metal cladding was employed, the samples were irradiated in the ungrounded and grounded conditions. KTFR was also tested on silicon-silicon oxide wafers.

Values up to 4000 volts were obtained for the metal clad ungrounded KTFR samples while values as low as 1 volt were obtained for the grounded samples. Similar measurements on HRP resulted in measurements as high as 242 volts and as low as 2 volts. KTFR with no metal cladding was measured as high as 13,000 volts while HRP was measured at 66 volts. Unusual charge distributions were obtained on the silicon samples.

Charge distribution profiles and charge decay curves were measured and recorded for the various samples.

CHARGE STORAGE ON
EMULSION AND PHOTORESIST
IRRADIATED BY AN ELECTRON BEAM

by

Arthur Kenneth Kreider

A Thesis

Presented to the Graduate Committee

of Lehigh University

in Candidacy for the Degree of

Master of Science

in Metallurgy and Materials Science

Lehigh University

1971

CERTIFICATE OF APPROVAL

This thesis is accepted and approved in partial fulfillment of the requirements for the degree of Master of Science.

MAY 5, 1971
Date

David A. Thomas
Professor in Charge

G. P. Cavard
Chairman of the Department of
Metallurgy and Materials Science

ACKNOWLEDGEMENTS

I wish to express my thanks to Professor D. A. Thomas of Lehigh University for his guidance in this endeavor. In addition, I wish to thank the members of Western Electric Research Center for their assistance, in particular, Peter D. Parry. Other members of the staff to which I am indebted are Messrs. G. I. Robertson, B. Weissman, K. H. Cho, T. J. Dewees and P. J. Sinclair.

TABLE OF CONTENTS

TABLE OF CONTENTS (Cont'd)

LIST OF TABLES

LIST OF FIGURES

LIST OF FIGURES (Cont'd)

ABSTRACT

Surface potentials have been measured on photosensitive materials after irradiation by an electron beam. Kodak HRP emulsion was irradiated with 6.2×10^{-9} coul/cm^2 and an order of magnitude above and below this value. Kodak KTFR was similarly irradiated at, above and below 6.2×10^{-6} coul/cm^2. Both materials were irradiated with 5, 10 and 15 KV electrons.

The resulting potentials were measured with a Kelvin Probe device featuring synchronous detection, phase adjustment and continuous data output.

The photosensitive materials were evaluated on glass substrates, with and without metal cladding on the glass. When metal cladding was employed, the samples were irradiated in the ungrounded and grounded conditions. KTFR was also tested on silicon-silicon oxide wafers.

Values up to 4000 volts were obtained for the metal clad ungrounded KTFR samples while values as low as 1 volt were obtained for the grounded samples. Similar measurements on HRP resulted in measurements as high as 242 volts and as low as 2 volts. KTFR with no metal cladding was measured as high as 13,000 volts while HRP was measured at 66 volts. Unusual charge distributions were obtained on the silicon samples.

Charge distribution profiles and charge decay curves were measured and recorded for the various samples.

INTRODUCTION

The electronics industry currently utilizes photolithography as a means of producing the small complex patterns required for integrated circuit manufacture. Present technology incorporates large scale drawings with photographic reduction[1]. Patterns for silicon I.C.'s, for example, are drawn to approximately 250 X final size, reduced initially on a large reduction camera and then further reduced on a step and repeat camera[2].

The precision requirements of patterns necessary for improved high frequency performance, better yields, and higher packaging densities approach the capability limits of the photographic process. The effects of diffraction and lens aberrations limit the minimum width of lines and spaces that can be produced over the required field (usually 2 inches by 2 inches). Electron beam irradiation has been suggested as a substitute for the photographic process[3].

Comparison of Conventional Photolithography and Electron Beam Processing

The processes of contact printing utilizing light microscope alignment was compared to electron beam irradiation[4]. Diffraction problems were observed when mask-to-slice separation exceeded 1 μm in the light process. Separations of 5 μm frequently occur during manufacture. The short wavelength of the electron beam (4000 $\mathring{A}$ for light versus .1 $\mathring{A}$ for 20 KV electrons) eliminates these diffraction problems when the electron beam process is employed. The depth of focus was found to increase from 7 μm for light to approximately

50 μm for the electron beam under the same conditions. The electron beam process is also considerably faster than the step and repeat method required in photoreduction. The advantages of the electron beam over light are discussed in detail by Samaroo, Broyde and Sagal[5].

One of the most important applications of the electron beam would be processing directly on semiconductor materials without the use of a mask. This technique is referred to as "direct circuit processing" in this report. The electron beam process should be superior to photolithography in the production of high resolution patterns.

Typical Electron Beam Exposure Apparatus

The electron beam process consists essentially of a beam of electrons guided over the surface of a flat sample of photosensitive material. Figure 1 shows a cutaway view of an Electron Beam Machine (EBM) that was developed for electron beam patterning. The electron optical column consists of an electron gun with re-entrant Wehnelt cylinder, focusing lenses and a deflection system. The gun produces a beam of electrons appoximately 50 μm in diameter. The lenses are adjusted to focus the electrons on the target (photosensitive material). A final beam size of 4 μm diameter and currents from 10^{-11} to 10^{-8} amperes are possible when the machine is operated at 15 KV.

The work area consists of a chamber with turntables to hold the photographic plates. The entire column and work area is evacuated

to about 5×10^{-5} torr with an oil diffusion pump with a liquid nitrogen baffle and a mechanical backing pump.

The beam is moved by an electrostatic or magnetic deflection system. A program for the desired pattern is printed on tape and serves as the input to the computerized deflection system. This data is converted on a digital to analog converter and activates the deflection plates. The electron beam then sweeps across the photosensitive material producing the desired pattern.

Photosensitive and Electron-sensitive Materials

The primary photosensitive materials employed in integrated circuit pattern generation, whether by photolithography or electron beam processes, are silver halide emulsions and photoresist. The emulsion is utilized in mask manufacture while photoresist is employed for processing on the semiconductor material.

The emulsions are essentially a dispersion of silver halide crystals in an organic gelatin[6]. The gelatin serves as a base for the halides and usually contains sensitizing agents necessary to the photographic process. The latent image formation is a function of the radiation (light or electrons) on the silver halide grains in the presence of the gelatin. The characteristics (sensitivity, resolution, etc.) of the emulsion are basically dependent on the relative proportions of the organic constituents and the size of the silver halide crystals. The exact reaction initiating the formation of the subsequently insoluble latent image is not presently known.

Photoresists are synthetic polymers in an organic carrier. Negative resists become insoluble when irradiated while positive resists become soluble. Negative resists, such as Kodak Thin Film Resist (KTFR) find the most frequent application. W. Kornfeld[7] suggests the insolubility of negative resists is primarily dependent on the interaction between the radiation and synthetic polymers in the organic solution. According to Charlesby[8], this interaction between electrons and polymers produces cross-linking and degradation of the organic molecules. The amount of cross-linking and degradation is affected by the dose and energy of the radiation. The response of photoresists may be improved by the addition of certain metal organic compounds and some readily dissociated materials. B. Broyde[9] has shown the addition of dibutyltin maleate to Kodak Photo Resist (KPR) reduced the dosage necessary to insolubilize a 4000 $\mathring{A}$ thick film from 9 to 2.5×10^{-6} coul/cm^2 while the addition of hexaphenyldilead to KTFR reduced the required dose from 7.5 to 1.5×10^{-6} coul/cm^2.

Surface Potential

Subjecting a material to irradiation by an electron beam usually results in the formation of a surface potential in the vicinity of the radiation impingement[10,11,12,13]. The presence of local surface potential can disrupt the precisely controlled deposition of electrons by deflecting the beam. An example of this distortion is shown by Munakata, Kohno, Maekawa, Honda and Miura[14]. They demonstrated a

trapezoidal distortion during the anticipated formation of a rectangle and attribute this distortion to the potential field effects of deposited electrons on incoming electrons. The accumulation and decay of this surface potential will be the major subject of this thesis. In addition to determining the magnitudes of any surface potentials, the rates of accumulation and decay may add information to the knowledge of the effects of the radiation on the emulsion and photoresist.

The surface charge can be measured with a device known as a Kelvin Probe. While originally designed to measure contact potentials this device can measure any surface potential without touching the surface of the specimen. Proper design of the probe allows it to be used as a scanning device before and after radiation. A profile of the charge on a sample can be developed. The shapes of the profiles and magnitudes of the charge will be determined.

EXPERIMENTAL PROCEDURE

Sample Materials

The primary goal of this investigation is to determine the effects of charge storage on materials commonly used throughout the semiconductor industry. Good examples of these materials are Kodak KTFR (Kodak Thin Film Resist) a photoresist, and Kodak HRP (High Resolution Plates), an emulsion. Both of these materials may be applied to various substrates. The HRP emulsion, for instance, is available on film (Estar Polyester Base), plastic and glass. For integrated circuit application it is most desirable to utilize the materials on a glass substrate for mask manufacture. The glass provides not only the required transparency, but also supplies a rigid flat working surface. Glass plates are available with a 3.5×10^{-5} in/in flatness tolerance. The substrates utilized here are 1/4 inch thick, 2-1/2 x 2-1/2 inch glass for HRP and .060 inches thick, 2 x 2 inch glass for the KTFR. Both these types of samples would be suitable for Electron Beam Machine processing.

Various techniques of applying the photosensitive materials to the glass substrates may produce different thicknesses. Both KTFR and HRP may, in fact, be purchased by a Kodak customer and applied to a thickness desired by the customer. In an effort to exercise some control over the application parameters, most of the samples were purchased from Kodak already deposited on a surface. Where this arrangement was not convenient, the photoresist was

applied in an appropriate manner. The Kodak KTFR samples were measured as 2800 Å and the laboratory prepared samples were 6000 Å. The HRP samples were approximately 40,000 Å.

Processing with masks has been improved by utilizing a chromium underlay on the glass substrate[15], beneath the photoresist or emulsion. Typically a 700 Å thick layer of chromium may be deposited on the glass substrate. Although originally designed to improve edge acuity and line resolution, the presence of a chromium underlay could certainly affect the distribution of charges on the surface of the material. Since this metallic underlay may affect the surface potential, samples with and without it were evaluated.

In the direct processing application, photoresist is applied to the oxide surface of the semiconductor material and patterned with the electron beam. Since direct circuit processing is a desirable accomplishment of the EBM process, samples of silicon-silicon oxide wafers were coated with photoresist and evaluated. The material utilized was arsenic doped silicon with a 1243 Å thick oxide layer. These parameters are typical for MOS device manufacture.

Summarizing, then, the materials to be evaluated will be Kodak KTFR and HRP. They will be evaluated with and without a chromium underlay. If the underlay is present, the materials will be tested as grounded and ungrounded. The KTFR will also be evaluated on silicon oxide.

The Electron Beam Machine (EBM)

During mask manufacture, the EBM provides a 4 μm diameter beam that is directed over the work area by a deflection system. An estimate of the magnitude and decay of any resulting potential is the goal of this investigation. A measurement of the charge in a 4 μm wide line is impossible by the method to be employed here. A much wider line is drawn and the value of this charge estimated. The results, then, are expressed as the potential produced by a given density of electrons per unit surface area.

The EBM employed in this investigation utilized a Canalco gun assembly. An RCA 206527 Electron Gun Filament Assembly heated by a current of approximately 2 amperes supplied the electrons. A re-entrant Wehnelt cylinder located closely about the filament was maintained at a voltage level sufficient to provide initial focusing of the beam. The high voltage anode was situated in the gun approximately one inch from the filament. The electrons were accelerated towards the anode and focused by the Wehnelt cylinder so as to pass through a hole in the anode. The position of the filament-Wehnelt cylinder assembly with respect to the anode was adjustable in the X-Y directions to control the direction of the beam.

Frequently, two or three magnet lenses are incorporated in the EBM column for focusing the beam to a 4 μm diameter size. Since the beam utilized here was comparatively large (1/8" diameter), only one lens was included in the column. An adjustable aperture was

located in the lens housing beneath the lens windings to establish the final current density. The aperture was adjustable in the X and Y directions and, to a degree, located the point of impingement of the beam on the sample.

Obtaining the desired beam size and current flow simultaneously is not always possible by adjusting the filament current. If the gun is operated outside of certain filament current ranges, a multiple image will result and, if the current is too high, the filament may be destroyed. To produce a beam size and current within the range of the filament adjustments, the size of the aperture may be changed. This allows more or less electrons to remain in the beam. The lens can then be readjusted to correct the beam size.

To facilitate changing aperture sizes, each aperture holder had several different size apertures. The apertures were located in a line and spaced so that only one would be in the beam area at any time. The aperture was adjusted from outside the vacuum system. Aperture sizes of 1, 2 and 5 mils were utilized in this investigation, giving intensity ratios of 1:4:25.

A magnetic deflection system was utilized for these experiments and is located beneath the lens apparatus. In an EBM designed for manufacture, signals would be applied to the two sets of coils or deflection plates in the form of digitally controlled voltages to sweep the beam over the area to be exposed. This sophistication is not required for the evaluations undertaken here. It is not necessary, or even desirable to produce any kind

of complex pattern. In fact, the most desirable pattern is a straight line. The straight line should be 1/8 inch wide and a known distance long (an inch was found to be a satisfactory length). To provide this pattern, one set of deflection coils was used to control the Y position of the line and the other set to provide a continuous sweeping action at that position. The Y position was controlled through a battery and voltage divider circuit. A deflecting circuit and the necessary amplifiers were utilized to control the nominal X position, the length of the beam and the sweep frequency. A line one inch long was swept at a frequency of 750 times per second.

The beam diameter of 1/8 inch and the line configuration were chosen to reduce the possibility of missing the point of the beam impingement when the probe is swept over the sample after irradiation. This reasoning will become more apparent when the work chamber and probe design are discussed.

The work chamber in the system employed here consisted of a large (15 in. x 15 in. x 15 in.) sealed chamber with doors serving as two sides. The doors provided ample access to the chamber from either side. A porthole was located in the front of the chamber for visual observation. A rotating disc seven inches in diameter was located inside the chamber for mounting samples. The disc was originally designed for irradiating one specimen and then rotating another into position under the beam. The shaft for rotating the disc extended outside the chamber and could be used to control

the position of the specimen in the chamber in a circumferential direction as a function of voltage.

The entire column and work chamber is evacuated when the EBM is operated. Electrons cannot travel well in air and the filament would oxidize if the system were not evacuated. A mechanical backing pump and a diffusion pump with a liquid nitrogen cold trap were utilized to evacuate the system. All of the data was obtained from runs at 2 to 5 x 10^{-5} torrs.

The Kelvin Probe

The Kelvin Probe of the type used here was originally developed in 1932 by W. A. Zisman[16] as a method of measuring the contact potential difference between two metals. When two dissimilar metals are placed in contact with each other, electrons can lower their energy by dropping from the Fermi level of one metal to the lower Fermi level of the other. This flow of electrons will continue until equilibrium is established at which point the Fermi levels are equal. The resulting displacement of electrons creates a potential difference between the two metals. If, in place of joining the metals directly, the two metals are connected through a large resistor, the electron flow will still occur and a voltage drop will be developed across the resistor during the time the electrons move. When the electrons have reached equilibrium, no current flow and, hence, no voltage drop will be seen across the resistor. However, if the two metals are in the form of capacitor

plates and the spacing between them is varied, the electrons must obey the equations:

$$C = \epsilon \frac{A}{d}$$

$$Q = VC$$

If the contact potential V is constant and C is varied regularly, then:

$$\frac{dQ}{dt} = V \frac{dc}{dt} + C \cancel{\frac{dV}{dt}}^{0}$$

$$\frac{dQ}{dt} = V \frac{dC}{dt}$$

The expression $\frac{dQ}{dt}$ is, of course, current and it will develop a continuous AC voltage across the resistor connecting the two metals. In the original Kelvin Probe, contact potential is determined not be measuring $\frac{dQ}{dt}$, but by applying a voltage to one of the plates exactly equal and opposite to the contact potential. Then $\frac{dQ}{dt}$ is zero and the voltage drop across the resistor is zero. This is essentially a "null" method and is depicted in figure 2.

$$i = \frac{dQ}{dt} = V\frac{dC}{dt}$$

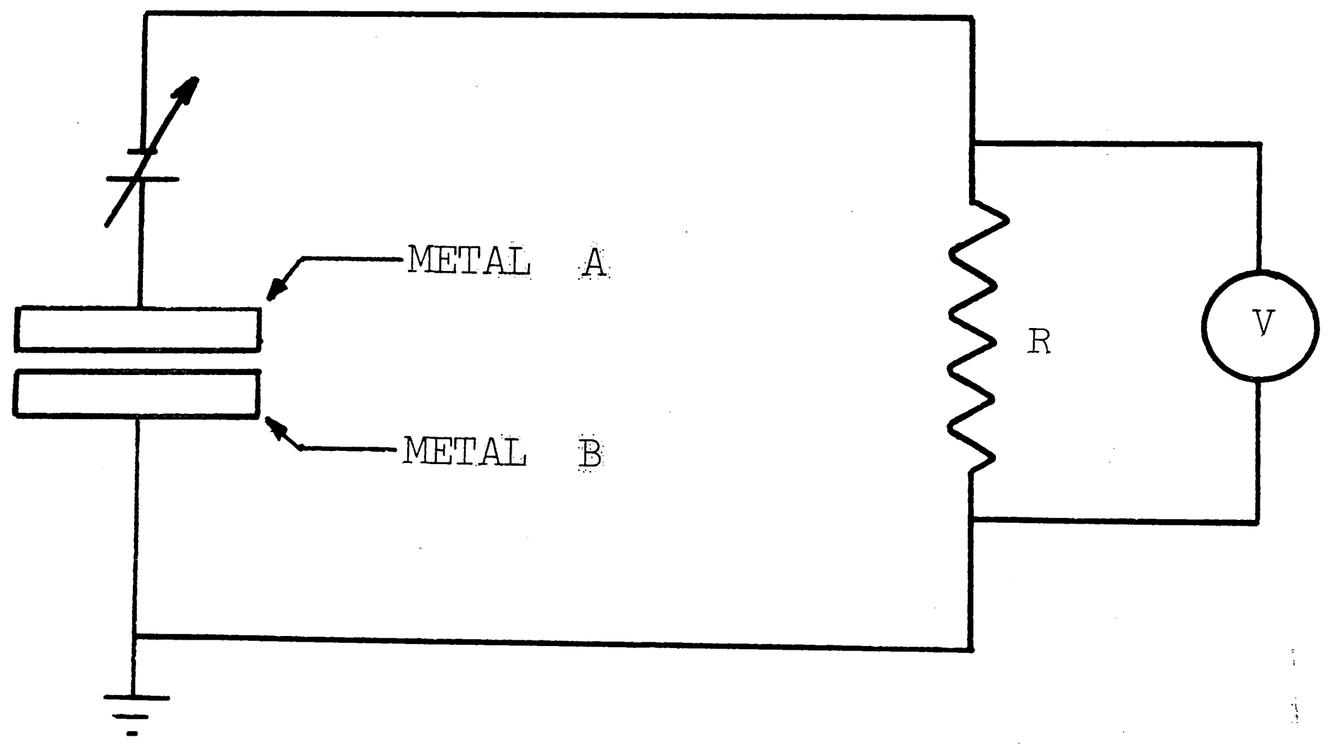

FIGURE 2 INITIAL KELVIN PROBE DESIGN

The apparatus was later refined by amplifying the signal across the resistor to more accurately determine the contact potential[17]. An important modification was recently made by Petit-Clerc and Carette[18]. Employing a synchronous detector and amplifier, they used a feedback from the amplifier to provide the bucking voltage that cancels the contact potential. The feedback bucking voltage was continually self-adjusting and could be monitored with a recorder. The synchronous detector is employed to reject ambient noise. The amplifier must incorporate a phase shifter so voltage of the proper sign is fed back.

The capacitance of a 1/8 inch diameter probe located .008 inches above the sample was calculated to be about .34 picofarads. To achieve good sensitivity, the shunt capacitance to the amplifier must be maintained at a low level. Towards this end, a bootstrapped Darlington circuit was mounted on the probe support. This current amplifier has unity gain and its proximity to the probe reduces spurious signal pick-up. A schematic of the current amplifier is shown in figure 3 and a diagram of the complete circuit is shown in figure 4.

These techniques are not confined to contact potential measurements, but will also measure surface charge. This is the type of apparatus used in this investigation to measure the charge stored on photoresist and emulsion.

The probe was attached to a telescoping boom that could swing in a large arc. The base of this structure was located on a set of X-Y micromanipulators. The probe could be manually positioned over the sample and final adjustments made with a micrometer to the nearest .001 inch. A photograph of the probe assembly installed in the chamber is shown in figure 5.

Investigators frequently employ electromagnets external to the vacuum system and elaborate mechanisms to transmit the vibrating motion to a probe located within the vacuum system. A modification to this concept was made in these experiments. The source of vibration was a earphone. It has the advantages of being simple,

inexpensive and easily used in a 10^{-5} torr vacuum. The probe was constructed from a Brandes "Admiral" Model BA-2 headset, a rigid nylon rod and a section of 1/8 inch diameter drill rod. The earphone was driven by a Hewlett Packard Model 2066 CD Signal Generator. The nylon rod was cemented to the vibrating metal disc of the earphone, and the drill rod inserted into the other end of the rod. The plastic retaining ring of the earphone was machined to fit over the assembly.

The AC signal developed across the large resistor was detected and amplified by a Model H.R. 8 Precision Lock-In amplifier manufactured by Princeton Applied Research Corporation. A reference signal was supplied to the Lock-In amplifier by the same H.P. Signal Generator driving the vibrating probe. The Lock-In amplifier has selective gains from .002 to 10,000 or in terms of sensitivity, full scale deflection from 500 millivolts to 100 Nanovolts. The phase of the reference signal and incoming signal is completely adjustable from 0° to 360°. An integral part of the amplifier is a DC output of 0-10 volts for full scale deflection. This output is used for the bucking voltage on the vibrating probe.

A Hewlett-Packard Model 4004A recorder is connected across the amplifier output to continuously monitor the surface charge.

A photograph of all the apparatus is shown in figure 6.

The probe was usually operated in a feedback mode as outlined above. This mode of operation is the most sensitive and provides a

certain degree of confidence. If the amplifier gain is sufficient and the phase angles properly adjusted, the magnitude of the resulting feedback voltage will balance the surface charge on the sample. This criterion can be presented in the form of a boundary condition equation as:

$$\text{AC signal} \times \text{gain} \times \text{ref. signal} \times \cos\theta \geq \text{Surface Charge}$$

where gain includes conversion to DC. If the above is not true, a measurement lower than actual will be observed. There is, however, an additional condition. The surface cannot exceed 10 volts because that is the maximum DC output of the amplifier. If the surface potential exceeds 10 volts the amplifier will simply saturate. Although this condition was not originally anticipated, it did occur and the measurement technique required modification.

The probe produces an AC voltage when moving in a potential gradient. The magnitude of the AC signal can be determined from measurements on the amplifier and indeed can be recorded as DC output. The DC output does not have to match the potential on the surface. The surface charge can be determined by knowing the relationship between the surface charge and the DC output.

The relationship between the AC signal developed and the DC output is merely multiplying the sensitivity times the phase angle

times the percent of full scale deflection. By monitoring the mixing circuit with an oscilloscope the angle can be maintained so that cos θ = 1. Reading the recorder output and knowing what sensitivity was selected provides the magnitude of the AC signal at the probe directly.

The problem, then, is determining the relationship between the potential on the surface and the AC signal developed. To establish this relationship an "artificial" charge was created on the sample to be irradiated by means of a power supply rather than bombardment by electrons. A DC power supply was attached to the sample and various voltages applied and the corresponding AC signal developed at the probe was measured. This technique, of course, can only be applied to those samples with a metallic underlay, but with these samples it works well. Potentials were applied up to 1400 volts. At 1450 volts, breakdown occurs. A calibration curve of volts (-DC) versus μV (AC) was developed for each sample. The results were used to estimate the magnitude of the charge on the surface of the sample after irradiation. The calibration curves were also utilized to estimate the charge on samples without a metallic underlay.

This concept of creating an "artificial" charge was also applied to check the operation of the circuit in the feedback mode. A potential was applied to the sample and the response of the recorder observed to assure the circuit was functioning properly.

An application of a 5-volt potential would result in a recorder measurement of 5 volts, the voltage being fed back to the vibrating probe.

Several parameters of the probe operation affect the voltage measured -

1. Amplitude - When the circuit is operated in the feedback mode, the amplitude of vibration must be great enough to provide sufficient feedback voltage to balance the surface charge. Without feedback the AC voltage developed will depend directly on the magnitude of vibration. On these experiments, the signal generator was maintained at 19.8 volts and the probe amplitude of vibration was measured as .0006 inches.
2. Spacing - The vibrating probe should be placed some optimum distance from the surface being investigated. If the probe is too close, surface irregularities and charge distributions become dominant effects. If the probe is too far, an inadequate signal is developed. Craig and Radeka[19] have evaluated this probelm. An equivalent circuit for the feedback mode is shown in figure 7.

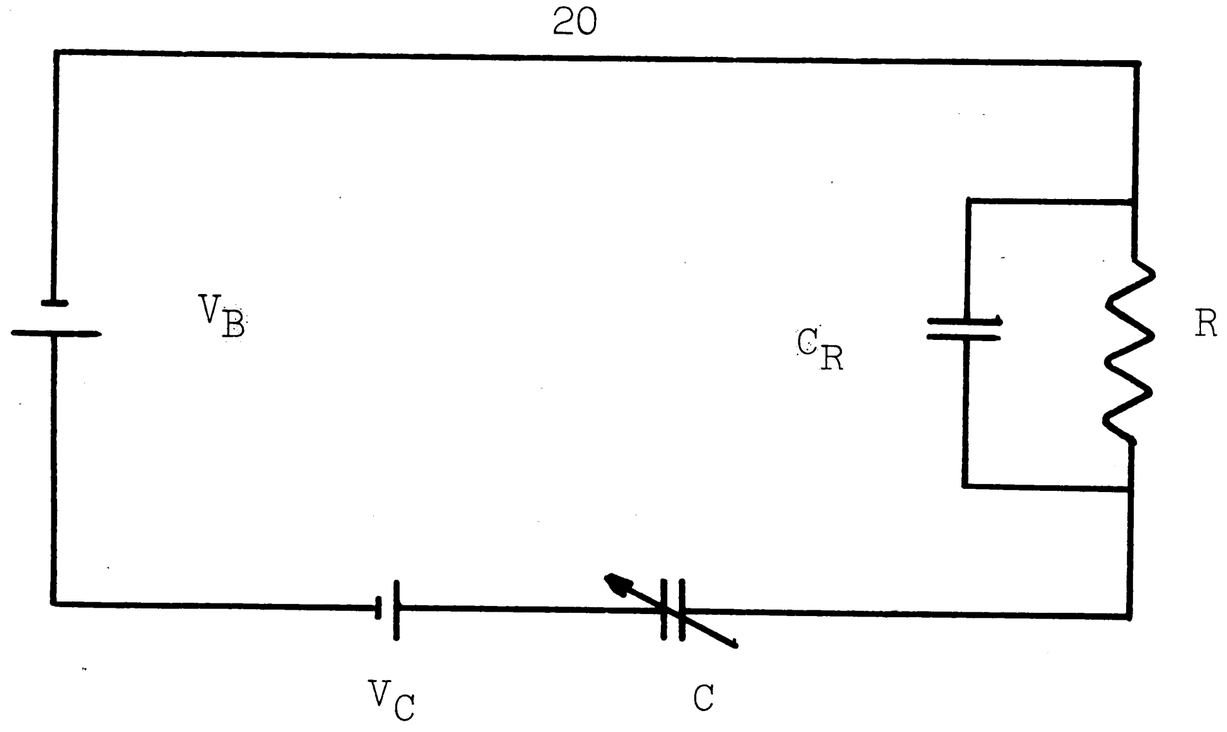

FIGURE 7 EQUIVALENT CIRCUIT FOR KELVIN PROBE

An equation for the AC signal developed may be written as:

$$V_{ac} = \epsilon (\Delta V_C - V_B - \beta V_{dc})$$

where ΔV_C = surface charge

V_B = bucking voltage

βV_{dc} = fraction β of DC output added to bucking voltage

$\epsilon = \frac{d \text{ (ampl. of vibration)}}{d_o \text{ (spacing)}}$; probe modulation index

Then, since $V_{dc} = \alpha V_{ac}$

$$V_{dc} = (\frac{\epsilon \alpha}{1+ \epsilon \alpha \beta}) \; x \; (\Delta V_C - V_B)$$

if $\epsilon \alpha \beta >> 1$

$$V_{dc} = \frac{1}{\beta} \; (\Delta V_C - V_B)$$

In these investigations $\beta = 1$ and $V_B = 0$, so:

$$V_{dc} = \Delta V_C$$

as desired.

To obtain the condition $\epsilon\alpha\beta \gg 1$, since $\beta = 1$, ϵ and α must be properly chosen. A gain of 200 was employed with a spacing of .008 to give a $\epsilon\alpha\beta$ value of: $\frac{.0006}{.008} \times 200 \times 1 = 16$. Since Craig and Radeka consider 10 sufficient, 16 should be adequate. The apparatus appears to perform well with these parameters in the feedback mode.

When the apparatus was not used in the feedback mode, the .008 inch spacing was maintained for both the calibration runs and sample evaluation.

3. Gain - When the DC output of the recorder is used at low gain values (without feedback), the effect of varying probe spacing becomes important. In some instances the probe was used in this mode to gain some knowledge of the charge profile of a sample charged to very high voltages. The resulting profile is not used to determine exact voltage level, but to estimate charge distribution.

4. Frequency - A frequency of 450 Hertz was employed.

Parameters

Electron Beam Machines are frequently operated at a high voltage level of 10 or 15 kilovolts. The system under study here is operated

at 15 KV while other electron exposure systems are designed to operate at 10 KV[14]. These two energy levels were investigated. In addition, since previous experiments indicate that photoresist could be more efficiently exposed at 5 KV, the 5 KV energy level was also investigated.

Emulsion and photoresist do not require the same dose level. Photoresists generally require a thousand times greater dose than emulsion. Typical emulsions doses are 5×10^{-9} coul/cm^2 and photoresist doses are frequently 5×10^{-6} coul/cm^2. In an attempt to evaluate the effects of the dose level on charge storage, each type of sample was irradiated with the previously mentioned dose, plus and minus one order of magnitude on each side. More accurately, KTFR was evaluated at dose levels of 6.2×10^{-5} coul/cm^2, 6.2×10^{-6} coul/cm^2, 6.2×10^{-7} coul/cm^2 at each of the three energy levels, 15 KV, 10 KV and 5 KV. HRP was evaluated at the same energy levels with doses of 6.2×10^{-8} coul/cm^2, 6.2×10^{-9} coul/cm^2 and 6.2×10^{-10} coul/cm^2.

The dose levels apply to a line 4 μm wide. That is, a line drawn by the movement of a 4 μm diameter beam. This dose was converted to a dose for a 1/8 inch wide line as follows: a beam of a certain current (electron flow) was repeatedly swept over a known distance for a prescribed period of time to provide the correct dose. A distance of one inch was selected as a convenient distance to sweep the beam. A current flow of 1×10^{-8} Amperes was selected for

irradiating the photoresist and 1 x 10^{-10} Amperes for the emulsion. These are the same current flows utilized in a mask-making EBM facility. The period of irradiation was adjusted to provide the correct dosage.

The electrons are deposited in a one-inch line to facilitate charge measurement. The sample must be irradiated under the beam and then rotated to a position under the probe. It would be extremely difficult to place a 1/8 inch diameter spot directly under a 1/8 inch diameter probe. The line generation was a solution to that problem. Actually, it also duplicates the real EBM process.

It should be noted, however, that since the period of irradiation is adjusted to provide the proper dose (and indeed varies from 5 seconds for the smallest dose on HRP to 83 minutes for the largest dose on KTFR), the rate of dose is a variable. Measurements were made to evaluate this effect.

To insure correct doses, the current flow was measured immediately before each sample irradiation. A Faraday Cup was located on the rotating disc inside the work chamber. The Faraday Cup serves as a device to measure all the electrons in a beam. A flat object would not count the primary and secondary backscattered electrons that leave the object after electrons of these energy levels strike the surface. The Faraday Cup is essentially a hollow cylinder, closed at both ends except for a small hole for the beam to enter. Only those electrons backscattered within the solid angle that describes

the entry hole are not counted and this is very few of the total. The Faraday Cup is insulated from ground and the beam current is read on a micromicroammeter connected to the Cup. A Faraday Cup is shown in figure 8.

Each time the energy level is changed the beam size changes. A method for measuring this parameter quickly and accurately was necessary. The beam size was determined by moving a copper plate with a square hole in it under the beam. The voltage from the potentiometer attached to the shaft of the disc was used to determine the distance the copper plate moved. An ammeter connected to the insulated copper plate was used to indicate when the beam entered or left the hole in the plate. The potentiometer output was applied to the X axis of a recorder and the ammeter output was applied to the Y axis. As the copper plate was rotated through the beam, the recorder would measure the current as a function of position. A sample result is shown in figure 9. The battery voltage supplied to the shaft potentiometer was 1.52 volts. The circumference of the circle on which the copper plate moves is 25.13 inches. The distance moved, then, is

$$\frac{\Delta S}{S_{circ}} = \frac{\Delta V}{V_{battery}}$$

$$\Delta S = \frac{S_{circ}}{V_b} \times \Delta V = \frac{25.13}{1.52} \cdot \Delta V, \quad \Delta S = 16.53 \times \Delta V$$

A plate with a 1/4 inch square cut-out was employed. If the beam is 1/8 inch diameter, no current flow would appear for 7.50 mv. That is,

$$\text{Beam Size} = .250 - \Delta S_o$$

$$.125 = .250 - 16.53 \times \Delta V$$

$$\Delta V = 7.50 \text{ mv.}$$

The recorder has a useful sensitivity of 2 mv/in with 10 divisions per inch. The points where current flow stop and begin can easily be read to $\pm$ 1/2 div. or .1 mv. The accuracy then is:

$$16.53 \text{ inches/volt} \times 2 \times 10^{-4} \text{ volts} = .0023 \text{ inches}$$

The appearance of the curves generated while the plate is moved through the beam is useful also for studying the density and symmetry of the beam. The actual shape of the slopes as the beam leaves or comes to an edge involves the convolution of circles and lines and will not be dealt with here. But, obviously, the curves under both conditions (opposite sides of the beam) should look alike. The copper plate can be seen in figure 8.

A plastic sample holder was fabricated to securely hold the samples. It is pictured also in figure 8. The plastic construction allows the sample to be electrically isolated from ground. An alligator clip and lead wire were used to ground the specimen when desired. The clip penetrated through the photosensitive surface.

A voltage regulator was utilized with the gun filament supply to stabilize the beam. The beam appeared stable within 5 percent for 30 minutes at the current levels employed.

The parameters are summarized in Table I.

Testing Procedure

To obtain results in the most useful forms, the following procedure was employed.

1. Feedback Mode - The sample was secured in the sample holder and initially connected to an adjustable battery voltage. The system was then evacuated and the sample was set at various potential levels within the range expected subsequent to irradiation. The response of the amplifier output and recorder were checked and adjusted if necessary. The battery was then disconnected and the sample grounded. These connections are external to the vacuum system and reach the sample through vacuum tight connectors installed in the work chamber.

   The beam is then turned on and the Faraday Cup moved under the beam. The filament voltage is adjusted to obtain the correct current flow. The deflection system was then activated.

   The sample was rotated under the beam, observing the shaft potentiometer output for positioning. After the prescribed exposure, the beam was turned off, a stop watch started and the sample rotated to a position under the probe.

Initially, a charge profile was obtained by sweeping across the entire sample. After sweeping the sample, the probe was placed over the point of interest on the sample (as determined on the recorder by the profile) and the recorder switched to a time base mode. The charge decay at the point of interest was then recorded as a function of time.

2. No Feedback - A similar procedure was followed here except the battery voltage applied was of a much greater magnitude and the sample was left ungrounded while being irradiated and tested. The calibration curve determined by applying the potential was initially generated by observing the AC signal value on the amplifier meter. Refinements as the experiments proceeded allowed the calibration to be measured as recorder response. All measurements (before and after irradiation) in this mode were taken at the same point to eliminate error due to changes in the probe-sample spacing due to surface irregularities.

3. Miscellaneous -

a) all parameters were recorded on a standard form for each sample.

b) silicon slices were not grounded with clips. An aquadag solution (an aqueous suspension of fine carbon particles) was used to paste the slice to the sample holder. A path of solution was formed to a fastening screw in one corner of the holder and the ground wire attached here. This afforded good contact.

RESULTS

The data from the charge measurements were obtained in two basic forms. A charge distribution profile was generated by sweeping the entire sample under the probe immediately after irradiation. After establishing the shape of the charge distribution, a point of interest was selected for decay measurements. The probe was located over that area (as seen by recorder position) and the recorder operated on a time base. In some cases, profiles of the entire sample were recorded at convenient time intervals. The data, then, appear as curves of charge distribution and charge decay.

The charge distribution was similar for certain conditions. In the grounded condition, all the metal-clad samples indicate relatively low potentials and clearly show the area of beam impingement. The ungrounded metal-clad samples appear as deep uniform wells at high potentials. As soon as the probe reaches the edge of the sample, it indicates a large negative voltage and continues to indicate approximately the same potential as the probe sweeps across the sample. It is difficult to detect the area of impingement on these samples. The low gain values required to record the high voltage levels makes the detection of relatively small variations difficult. The profiles observed for the samples without metal cladding indicate clearly the point of impingement, although the charge seems to have spread over a larger area. The silicon samples behave in much the same manner as the KTFR

samples. A summation of the charge distributions for the various conditions is presented in figure 10. No attempt is made to indicate actual voltage.

The decay curves for KTFR and HRP are plotted on semi-log paper. The curves for an energy level of 15 KV appear as figures 11 and 12 respectively. It is obvious that the ungrounded metal clad samples charge to a much greater potential level than the grounded samples. As might be expected, the samples charged to the highest potential decay at the fastest rate. The decay times are plotted for 30 to 50 minutes for the various samples. The time required to record the charge distribution profile frequently prevented the recording of points near t = 0.

There appeared to be little difference between the results obtained at 15 KV, 10 KV or 5 KV energy levels. To indicate the similarities, the decay curves for ungrounded KTFR with the same dose level (6.2×10^{-6} coul/cm^2) and energy levels of 5, 10 and 15 KV are plotted on the same graph as figure 13. Curves for the charge decay on grounded HRP with the same dose level (6.2×10^{-9} coul/cm^2) and energy levels of 5, 10 and 15 KV are also plotted together as figure 14.

An exception to this rule occurred in the irradiation of grounded KTFR at 5 KV. Under these conditions, a much greater charge was apparent than at the 10 KV and 15 KV levels. A comparison of the effects of the energy level is seen in figure 15.

One of the most interesting observations was the appearance of a positive node in the profile of the charge distribution of the grounded KTFR samples. The node appeared at all dose levels at the 10 and 15 KV energies. While it could not easily been seen at 5 KV, there were indications that it did occur there also. The magnitude of the positive node was frequently great enough to produce a total resulting potential that was positive. Subsequent profiles obtained during the charge decay indicate the positive peak becomes reduced. An example of this phenomenon is shown in figure 16. All the decay curves for KTFR were obtained from the most negative point on the profile. To indicate the presence of this node a decay curve was acquired for the peak. A curve from a 10 KV sample is shown in figure 17. The HRP material did not exhibit this effect.

The vacuum pressure appears to greatly influence the charge decay rate. Although no attempt was made to evaluate this parameter in detail, figure 18 shows the effect of opening the system to atmospheric pressure while charge decay was being measured.

The silicon wafers coated with KTFR produced results that were, in some aspects, similar to the results from KTFR on glass with a metal underlay. The magnitude of the positive peak on the grounded silicon sample appeared to be greater than occurred on glass and the areas of the wafer not irradiated appeared to be at a uniform negative potential. The positive charge on the silicon did not

decay rapidly, even when the system was open to the air. In fact, the sample changed little over a 24-hour period at atmospheric pressure. Profiles obtained 24 hours apart are shown in figure 19. The ungrounded silicon samples acted like unclad KTFR samples.

In anticipation of annealing the silicon sample to measure the effects of annealing on the charge storage, the KTFR was removed. Acetone was used to remove the resist. Before annealing, the sample was rechecked and the charge appeared to be completely gone. Profiles before and after the resist removal are shown in figure 20.

An attempt was made to measure charge storage on the silicon wafer (grounded) with no resist coating. After extensive radiation no effects could be detected.

An attempt was made to evaluate the effects of the rate of irradiation. A sample of KTFR was irradiated with a dose of 6.2×10^{-6} coul/cm^2 at an energy level of 15 KV. The sample was initially irradiated with a current of 1×10^{-8} amperes for 500 seconds. As a comparison, a sample was irradiated with a current of 8×10^{-8} amperes for 62.5 seconds. No difference was observed beyond the limit of experimental accuracy. The profile for these samples are shown in figure 21. KTFR was chosen for evaluation because of the appearance of the positive peak. It was thought that this peak might be sensitive to the dose rate and

it would be easy to observe any difference. Broyde[9] does say that photoresists show reciprocity for current density and time. This data would substantiate that supposition.

Since the magnitudes of the charge on any sample could not be measured at t = 0, a regression analysis was performed and the t = 0 intercept was determined. The data for the intercept included only the first 3 or 4 points. It was assumed the decay curves obey an exponential equation so a logarithmic regression was performed. Assuming those curves that change slope could be process activated by two or more driving forces, the rate constants at the beginning and end of the measured decay were calculated. Table II summarizes the expected peak values and the rate constants. The first values of V_o (surface potential-volts) and A (rate constant-reciprocal minutes) are near the t = 0 intercept. The second values are taken where the slope of the curve appears to be constant; that is, where $t \approx 50$ minutes.

DISCUSSION

Magnitude of Stored Charges

One of the most important results of these experiments is the determination of the magnitude of the surface potential on photosensitive materials when they are irradiated with an electron beam. As can be seen from either the decay curves or the data in Table II, values of hundreds and thousands of volts were measured. The metal clad ungrounded KTFR, for instance, was measured at a potential of 2600 volts one minute after irradiation. The magnitude of these potentials makes them important.

The magnitude of the surface potential will be discussed for each set of conditions.

1. Metal Clad, Ungrounded - the shape of the profiles and the relative potential levels suggest the magnitude of the surface potential is a function of the number of electrons irradiating the sample. The electrons apparently strike the sample and then spread out over the surface of the sample in an even distribution. This type of distribution was observed on all the ungrounded metal clad samples and the ungrounded silicon wafer samples.

A comparison of the ungrounded KTFR samples in figure 11 with the ungrounded HRP samples in figure 12 indicates the KTFR samples charge to a higher potential than the HRP (see also Table II). This is probably not a function of the

material but a measure of the total number of electrons striking the sample. The dose on the KTFR is, on the average, 3 orders of magnitude greater than the HRP dose. If the materials themselves contribute to the magnitude of the potential, it is probably through such characteristics as electron backscattering coefficients and conduction.

The potential dependency on dose is further illustrated in figure 13. These curves indicate that dose determines the potential and that energy has little effect on the resulting potential.

It is obvious that increasing the dose increases the resulting surface potential. If the surface potential is a direct function of dose alone, then since the dose was varied over three orders of magnitude for each sample, the surface potential should vary over the same magnitudes. The data does not indicate that it does. There are several reasons why this may not occur. An important consideration is the effect the potential field established by electrons previously striking the surface has on incoming electrons. Certainly the first electrons striking a sample that is at zero potential respond differently than an electron that attempts to strike the sample when it is at a several hundred or thousand volt potential. Quite possibly, the secondary yield may increase as the potential of the sample increases,

resulting in proportionately fewer electrons remaining on the sample.

If this were the only effect, the curves would merely become closer together as the dose is increased. That this occurs is not obvious from the data, however, three values of dose may not be sufficient to clearly demonstrate the effect.

Another factor may be voltage breakdown along the edge of the sample. If the local electric field exceeds breakdown value, microdischarge will occur, limiting the maximum potential.

Theoretically, the isolated sample could charge to the same level as the energy of the electron (5, 10 or 15 KV). If one of the above or some other factor does not limit the maximum value of the potential this may indeed occur. This would mean that the potential of a metal clad ungrounded glass plate employed in mask generation (or an ungrounded silicon slice in direct circuit processing) would be dependent on the energy of the beam and the dose and the density of the pattern. This last factor is a consequence of the relationship between the surface potential and the total number of electrons striking the sample.

2. Metal Clad, Grounded - the profiles recorded for this condition indicate a localized effect in both KTFR and HRP.

As opposed to the magnitudes of the ungrounded conditions that were never measured below 40 volts, these magnitudes do not exceed 20 volts and most are less than 10 volts. For the same beam and sample conditions and only the ground varied, the potential is at least 2 orders of magnitudes less for the grounded condition. While both the KTFR and HRP show the localized effects when grounded (both show uniform distribution over the sample when grounded) the details of the effects are markedly different. As shown in figure 10, the HRP profile is a simple negative depression. The KTFR, however, shows a positive peak at the center of the negative depression. The absolute value of this peak can be positive, as was seen on a sample irradiated at 15 KV with a dose of 6.2×10^{-6} coul/cm^2. The relative height of this peak appears to increase with dose, however, the absolute value decreases as the dose increases because the level from which it begins is lowered. Profiles with absolute values of this peak positive are the results of a moderate dose.

The charge decay on this type of sample was not as simple as it was on the other samples. Not only does the negative charge decay, but the peak also decays. As a result of the peak decay, some points on the charge profile will become more negative with time. Eventually the peak disappears and the charge at that point decays towards zero voltage. Figure 16

is an example of the peak decay. It also indicates the relative potentials involved. The decay curves are normally plotted from data recorded at the lowest point on the profile. Figure 17 indicates the type of results obtained if the decay is measured from the top of the peak.

The charge distribution for KTFR on the silicon wafer also shows the formation of a positive peak. However, on this sample a uniform negative potential exists everywhere else on the sample. The absolute value of the peak is clearly positive.

Charge profiles of the nature discussed above indicate that more than just electron storage is occurring. The formation of potentials with absolute positive values suggests some contribution by the material itself. Possible mechanisms that could produce the observed results will be discussed in the next section.

3. No Metal Cladding - the storage on KTFR and HRP with no metal cladding differed from each other and both differed from the metal clad conditions.

The KTFR produced a profile with a magnitude similar to the ungrounded condition but still showed the positive peak effect as seen in the grounded condition. (See figure 10.) The fact that the entire sample drops to some negative potential level suggests that the electrons spread out (diffuse)

through the resist rather rapidly. The presence of the positive peak indicates the material is still making some kind of contribution to the charge distribution. The magnitude of the charge was initially surprising. When irradiated at 15 KV and 6.2 x 10^{-2} coul/cm^2, the ungrounded metal clad sample is at -385 volts while the sample with no metal cladding is at -2800 volts if both are measured two minutes after decay begins. One difference between the clad and not clad samples is the thickness. The photoresist on the metal clad samples was applied by Kodak and measured as 2800 A thick. The resist on the sample without cladding was applied in the laboratory and subsequently measured at 6000 A. This difference in thickness could be responsible for the apparent increased charge storage.

The HRP profile was similar to the grounded metal clad HRP sample, except the potential was somewhat greater. Under identical irradiating conditions of 15 KV and 6.2 x 10^{-8} coul/cm^2 the grounded metal clad sample is at a potential of -17 volts while the sample with no metal cladding is at -46 volts when measured three minutes after decay starts. The charge is spread over a wider area than in the grounded metal clad condition and indeed there are indications that the whole sample is becoming charged as in the ungrounded condition, similar to the KTFR.

Decay curves for KTFR and HRP with no metal cladding are shown in figures 22 and 23, respectively.

Charge Storage and Decay Mechanisms

1. Metal Clad Ungrounded Samples and Samples with no Metal Cladding - the accumulation or decay of the charge on photosensitive materials does not lend itself to rigid mathematical solution. For instance, the charge distribution on the metal clad ungrounded samples and the samples with no metal cladding should be largely a function of electron diffusion (conduction) in the material. The area where the beam strikes the sample would be at a large potential and create the potential gradient (field) necessary for the net transport of electrons away from that area. In some period of time after irradiation ceases, the charge should be uniformly spread over the sample. Such a picture is useful and probably reasonably accurate. However, an applicable mathematical model for the evaluation of measured parameters is not available.

The rates of electron diffusion in the photosensitive materials and in the metal cladding could be evaluated by comparing the HRP metal clad ungrounded sample with the HRP unclad sample. The electrons in the metal clad samples have two paths by which they can move. They can diffuse through the photosensitive material or they can move through the metal. In the unclad sample they can only move through the material. A comparison of the effects of these paths may be seen in the HRP profiles in figure 10. The metal clad

samples present a uniform profile immediately after irradiation while the unclad samples show a valley or depression at the point of impingement. This would indicate the electrons reach the metal and diffuse more rapidly in the metal.

If there were no other factors to be considered, the potential in the depression of the unclad sample should be greater than that of the clad sample. This is not substantiated by the HRP data. The rate of decay for the sample with no cladding may be a clue to the difference in accumulated charge. As can be seen by comparing the decay curves for HRP, the unclad sample decays at a much greater rate than the clad sample. The decay is not due to charge spreading. Repeated profile measurements show the potential decreasing everywhere. It is possible that the unclad sample may decay too rapidly to be measured or it may decay too rapidly to build to a high potential. The reason for this is not clear.

The clad and unclad KTFR samples cannot be directly compared because they have different thicknesses.

2. Metal Clad Grounded Samples - the grounded metal clad sample produces only local disturbances. Any model similar to diffusion equations would predict less charge spreading because the low potential in the area of beam impingement creates a relatively small potential gradient. The potential is minimized because the electrons cannot accumulate on the

sample. Indeed, the samples were grounded through an ammeter and as the beam was striking the sample, a current was measured that was approximately eighty percent of the beam current.

The exception to this rule is the KTFR sample irradiated with a 5 KV beam. The potentials measured for 5, 10 and 15 KV are shown in figure 15. This increase in stored charge could be a measure of the electrons' ability to penetrate the resist.

The following calculation is used to determine the depth of penetration in KTFR. An approximation to the Thomson-Widdington Law is[9]:

$$V^4 = V_o^4 - \left(\frac{16 \pi N_{ave} e^4 Z}{m^2 A} \cdot \frac{\ln mv^2}{I} \right) \rho x$$

where

V_o = initial velocity

A = average gram atomic weight

Z = material's average atomic number

I = material's mean excitation potential

m = electron mass

v = electron's velocity

e = electron charge

N = number of atoms/cc

ρ = material density

x = penetration distance in material

solving for x at V = 0

$$x = \frac{V_o^4}{\left(\frac{(16 \quad N^4 \quad Z}{m^2 \quad A} \cdot \frac{\ln m V^2)}{I}\right)}$$

for a 15 KV electron:

$V_o = .74 \times 10^{10}$ cm/sec

$Z/A = .51$

$I = 11.5$ ev

$\rho = .9$ gm/cm^2

$NZ = 3 \times 10^{23}$

and

$x = 1.07$ microns

For 5 KV, $x = 0.13$ microns

10 KV, $x = 0.5$ microns

15 KV, $x = 1.07$ microns

The KTFR samples are 2800 Å or .28 microns thick. The calculations suggest that most of the 10 and 15 KV electrons pass entirely through the KTFR and most of the 5 KV electrons are captured. The results here would seem to confirm the Thomas-Widdington Law as opposed to many other solutions for the penetration distance.

3. <u>The Positive Peak in KTFR</u> - the appearance of this peak suggests the redistribution of charges in the material proper. The writer proposes the peaks are the result of accumulation of positively charged ions. The ions are either in the resist initially or are a result of reaction between the resist and the electron beam. While the beam is striking the resist a large negative potential exists and the positive ions are attracted to that area. When the beam is turned off, the electrons creating the negative potential quickly disperse and the positive ions are left in position. They too will disperse, but at a much slower rate than the accumulation rate because the driving force (potential) is much less.

KTFR, a polymerized isoprene dimer of molecular weight 100,000, is insolubilized by free radical reactions like the following.

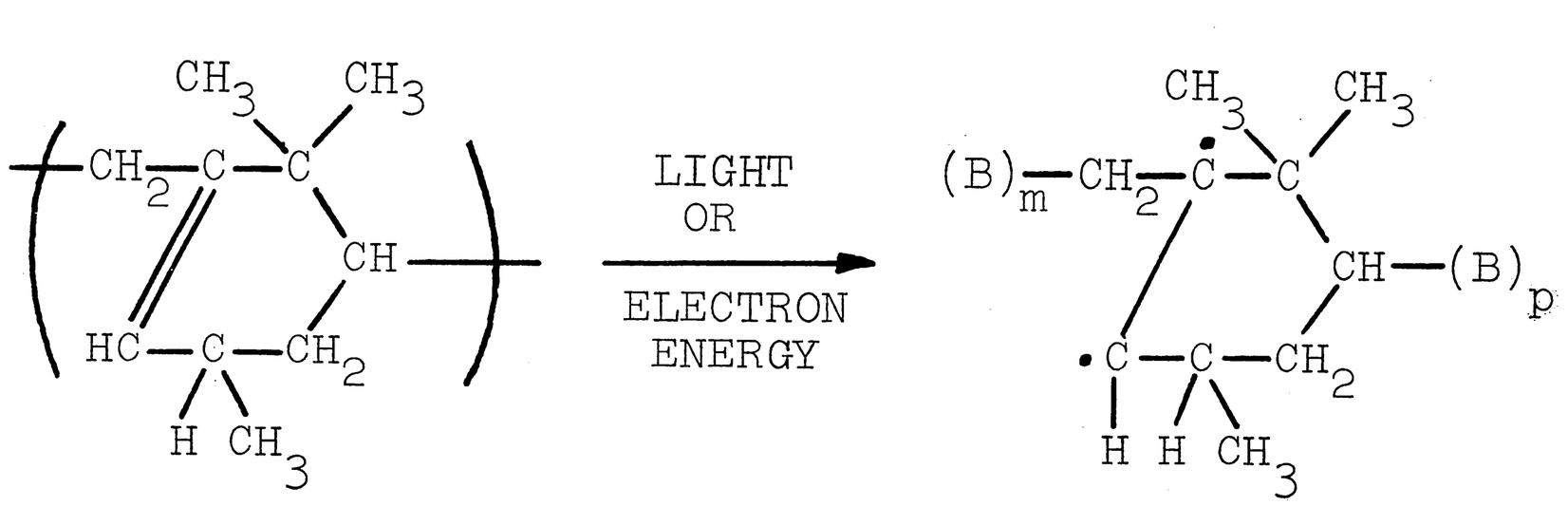

KTFR

A DIRADICAL

This diradical reacts with another KTFR molecule to give:

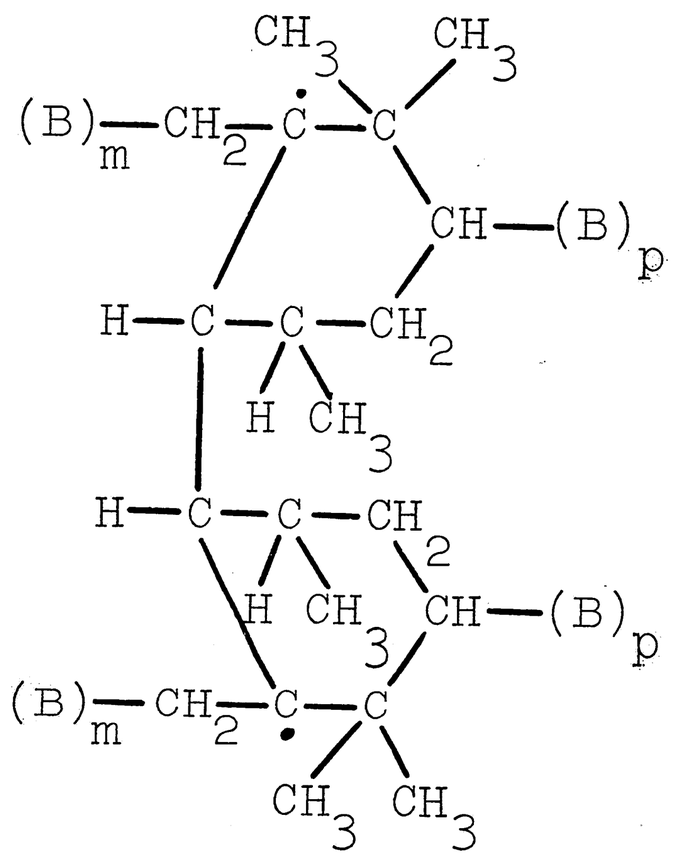

where B is the monomer:

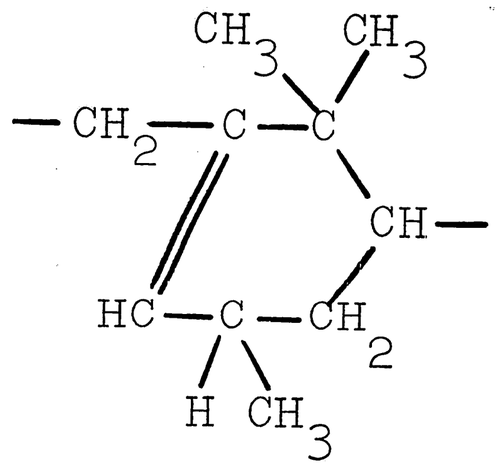

a diradical that can react further.

The purpose for presenting the reaction is to indicate the large number of hydrogen bonds in the molecules. The bond energies of the carbon-hydrogen bonds are of the order of 4 eV and the double carbon bonds are of the order of 5 to 6 eV. The 5K to 15K eV electrons have more than enough energy to break both these bonds. The insolubilization of the resist is proof that the C = C bonds break and if they break, then there is every reason to expect the C - H bonds to break[20]. Ordinarily the hydrogen ions would become re-bonded to the

carbon. However, in the presence of a large potential field they may move towards the field. The probe measures the hydrogen ions remaining in the area of the beam impingement after the beam is turned off.

Since the charge apparently redistributes itself, it may have no effect on subsequent processing of the resist.

A somewhat similar form of positive charge was observed by Petit-Clerc and Carette[18]. No attempt to explain it was made at the time.

4. Silicon Wafer Sample - the ungrounded silicon samples behave like the unclad KTFR glass samples. The potential is rather large (50-100 volts) and shows a more positive value in the center of the sample.

The grounded sample appears to possess the characteristics of both the grounded and ungrounded KTFR samples. This effect is probably due to the insulating effect of the silicon oxide layer on the wafer. This insulating material would make the KTFR behave as though it were ungrounded (or unclad, and there is not so much difference between the two) and results in negative potential on the entire surface of the sample. Since the silicon material under the oxide is grounded, and the beam has enough energy to penetrate the photoresist (these experiments were conducted at 10 and 15 KV), the uniform

potential would not be very large. It probably results from electrons scattered back into the photoresist from the silicon or silicon oxide layers. The relatively high diffusion rates in KTFR that resulted in a large negative potential over the entire glass sample in the unclad condition would also spread this smaller charge uniformly over the silicon sample.

The fact that the sample is acting as a grounded sample would result in the familar positive peak formation as is observed.

CONCLUSIONS

The results of this investigation indicate large surface potentials may be developed on photosensitive materials when they are exposed by the electron beam method. These potentials do not decay very rapidly. As a result, the shape of a pattern generated on the material could be affected.

The most desirable condition from the viewpoint of surface potential is metal clad grounded samples. The surface potential is reduced to a minimum under these conditions.

To obtain these conditions the photosensitive substrate would have to be acquired with a metal coating. Since present technology incorporates a metal layer for other reasons, this should be no problem.

Grounding the sample is also relatively simple. If some area of the sample is provided that is not necessary to the pattern generation, the holding device may be designed to scratch through the photosensitive material to the metal cladding. Grounding through an ammeter is a simple way to be sure the sample is grounded. An appropriate current reading on the meter during irradiation will indicate charge not accumulating on the sample.

The problem of irradiating silicon wafers with oxide surfaces is not so easily solved. If the charge never accumulates beyond the 5 volt level observed here, then grounding will work on the

silicon samples also. However, if the charge observed is a function of the oxide thickness or some other inherent characteristic of the material, charge may accumulate to a higher potential and some other solution may be necessary.

In conclusion, these experiments have been useful in determining the magnitude of the surface potential on photosensitive materials under typical irradiation conditions.

TABLE I

MATERIAL	KTFR			HRP			SILICON		
Dose (x 6.2 coul/cm^2)	10^{-5}	10^{-6}	10^{-7}	10^{-8}	10^{-9}	10^{-10}	10^{-5}	10^{-6}	10^{-7}
Energy: 15 KV	GUN	GUN	GUN	GUN	GUN	GUN	G	-	G
10 KV	GU	GU	G	-	G	-	G	G	GU
5 KV	G	GU	-		G	-	-	-	-

G = Metal Clad, Grounded

U = Metal Clad, Ungrounded

N = No Metal Cladding

TABLE II

ASSUMING EQUATION OF FORM: $V = V_o^{-At}$				
SAMPLE	NEAR t = 0		AT CONSTANT SLOPE	
	V_o	A	V_o	A
KTFR (metal clad)				
Ungrounded 15 KV				
6.2×10^{-5} coul/cm^2	4000	604	340	.043
6.2×10^{-6} coul/cm^2	650	89	190	.043
6.2×10^{-7} coul/cm^2	460	74	90	.058
Grounded 15 KV				
6.2×10^{-5} coul/cm^2	14.00	.050	4.35	.006
6.2×10^{-6} coul/cm^2	1.86	.017	1.73	.001
6.2×10^{-7} coul/cm^2	1.18	.013	1.07	.004
HRP (metal clad)				
Ungrounded 15 KV				
6.2×10^{-8} coul/cm^2	242	.044	150	.016
6.2×10^{-9} coul/cm^2	68	.025	50	.002
6.2×10^{-10} coul/cm^2	42	.018	37	.005
Grounded 15 KV				
6.2×10^{-8} coul/cm^2	17.40	.020	13.2	.008
6.2×10^{-9} coul/cm^2	2.41	.003	2.5	.005
6.2×10^{-10} coul/cm^2	2.18	.001	4.5	.0006

TABLE II (Cont.)

SAMPLE	ASSUMING EQUATION OF FORM: $V = V_o^{-At}$ NEAR t = 0 V_o	NEAR t = 0 A	AT CONSTANT SLOPE V_o	AT CONSTANT SLOPE A
KTFR (not metal clad)				
15 KV				
6.2×10^{-5} coul/cm^2	13,000	.400	2000	.016
6.2×10^{-6} coul/cm^2	3,750	.135	2800	.053
6.2×10^{-8} coul/cm^2	735	.248	350	.102
HRP (not metal clad)				
15 KV				
6.2×10^{-8} coul/cm^2	66	.133	400	.055
6.2×10^{-9} coul/cm^2	40	.365	16.3	.0013
6.2×10^{-10} coul/cm^2	33	.280	16.0	.0013
KTFR (metal clad)				
Ungrounded-6.2×10^{-6} coul/cm^2				
15 KV	600	.233	187	.044
10 KV	1050	.460	105	.035
5 KV	660	.184	170	.036
HRP (metal clad)				
Grounded-6.2×10^{-9} coul/cm^2				
15 KV	2.53	.006	2.5	.005
10 KV	1.72	.022	1.65	.015
5 KV	2.30	.014	2.05	.006

FIGURE 1

ELECTRON BEAM MACHINE

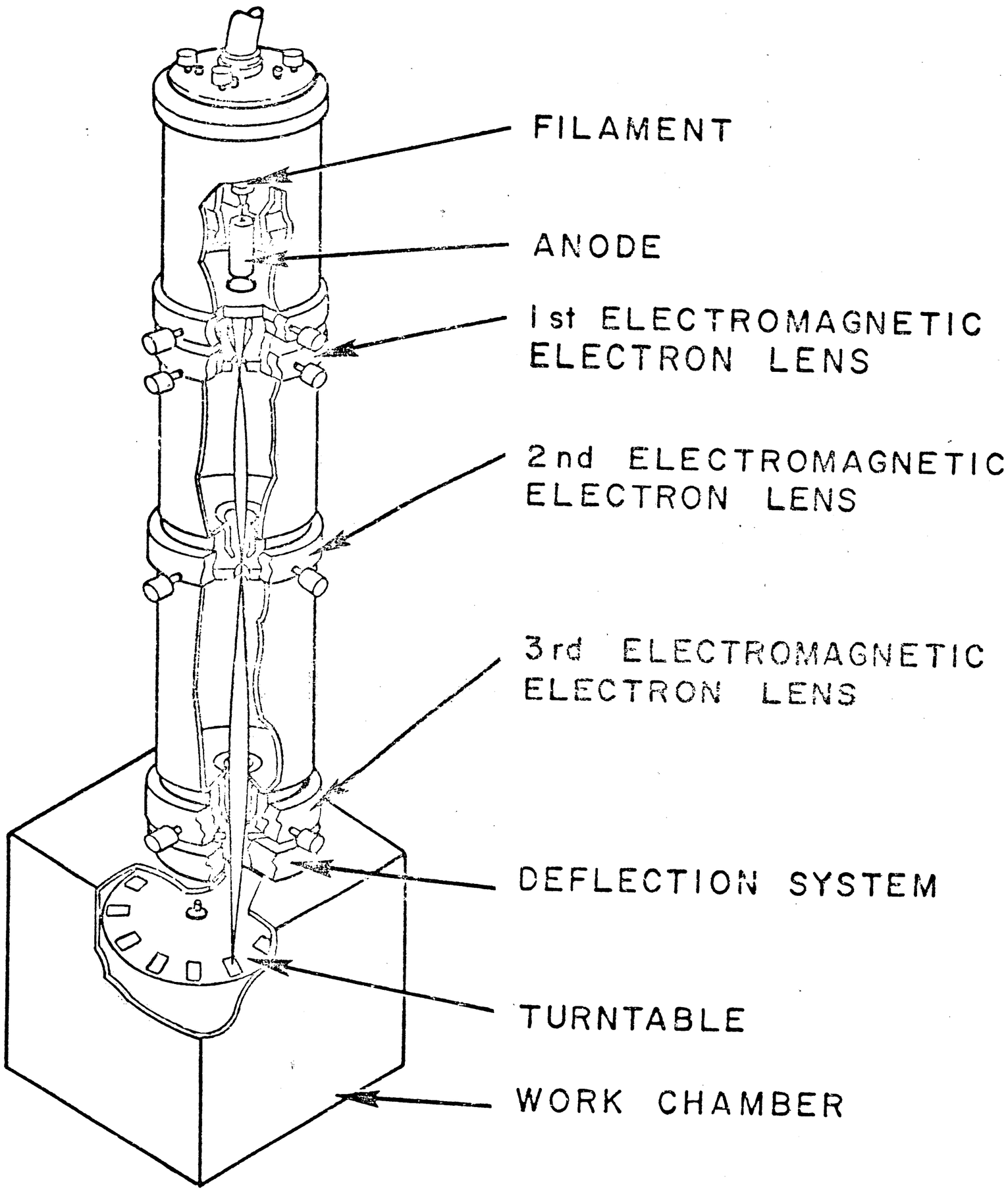

FIGURE 3
BOOTSTRAPPED DARLINGTON CIRCUIT
CURRENT AMPLIFIER

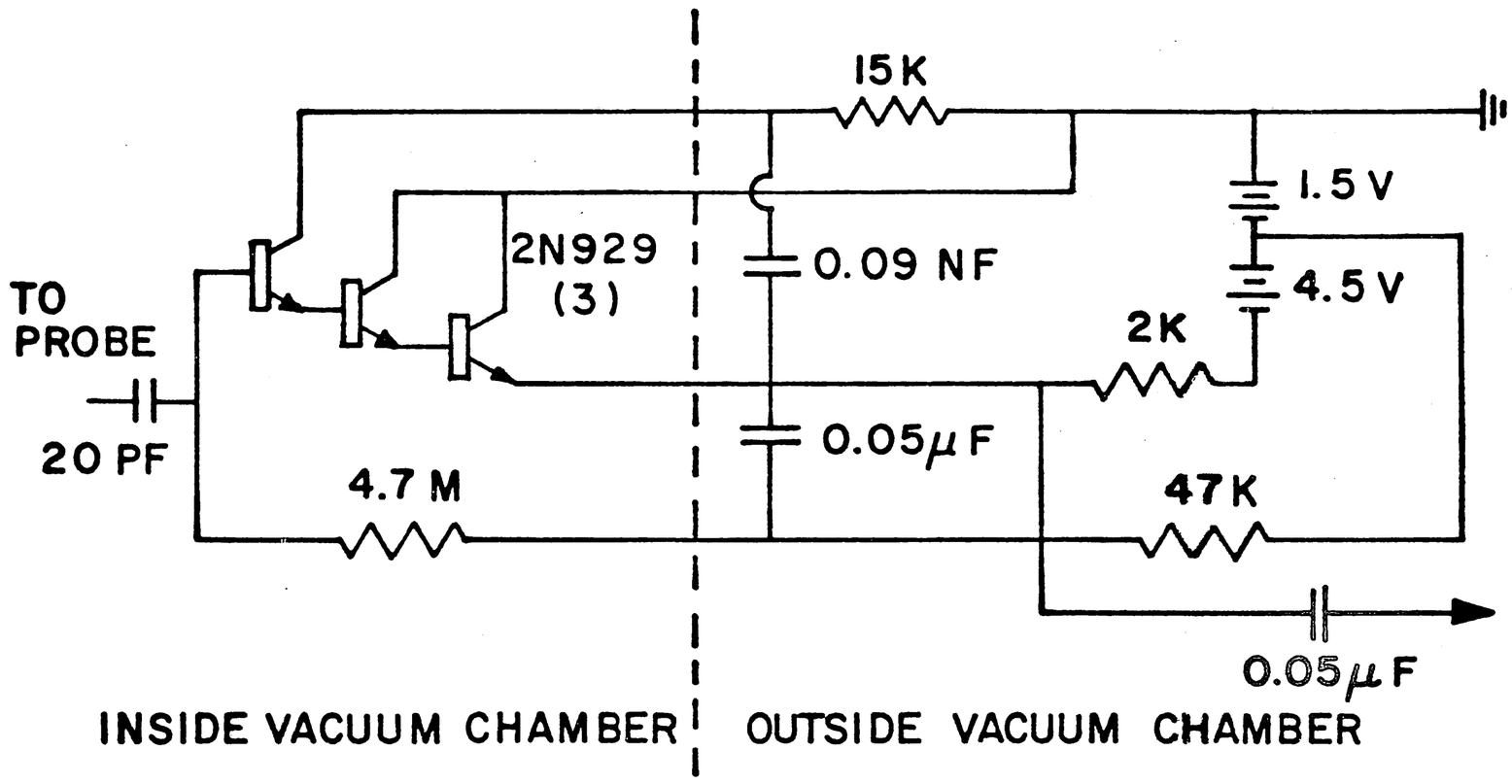

FIGURE 4
COMPLETE KELVIN PROBE

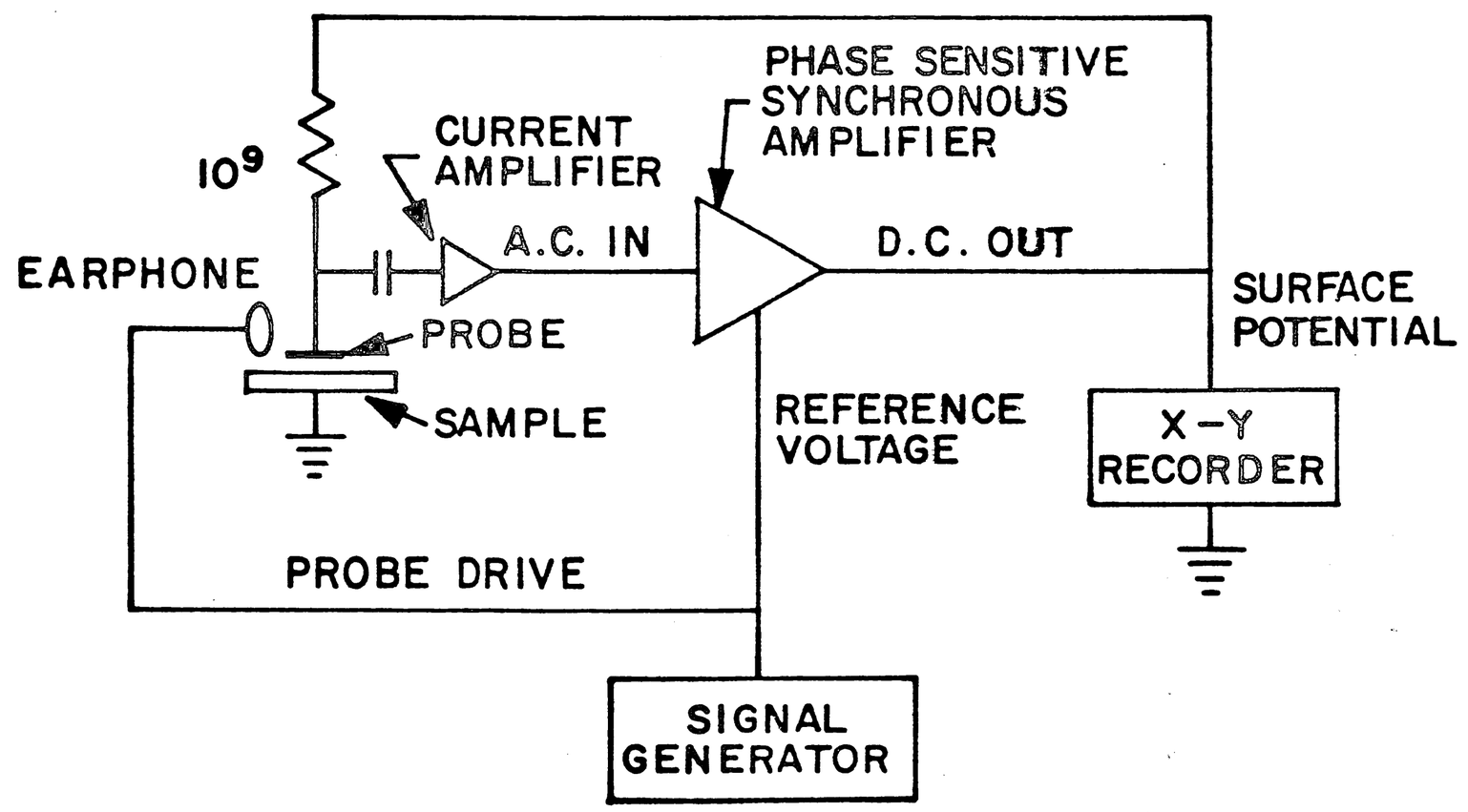

FIGURE 5

PROBE ASSEMBLY IN CHAMBER
EARPHONE IS ATTACHED TO TELESCOPING
BEAM. PROBE IS POSITIONED OVER SAMPLE

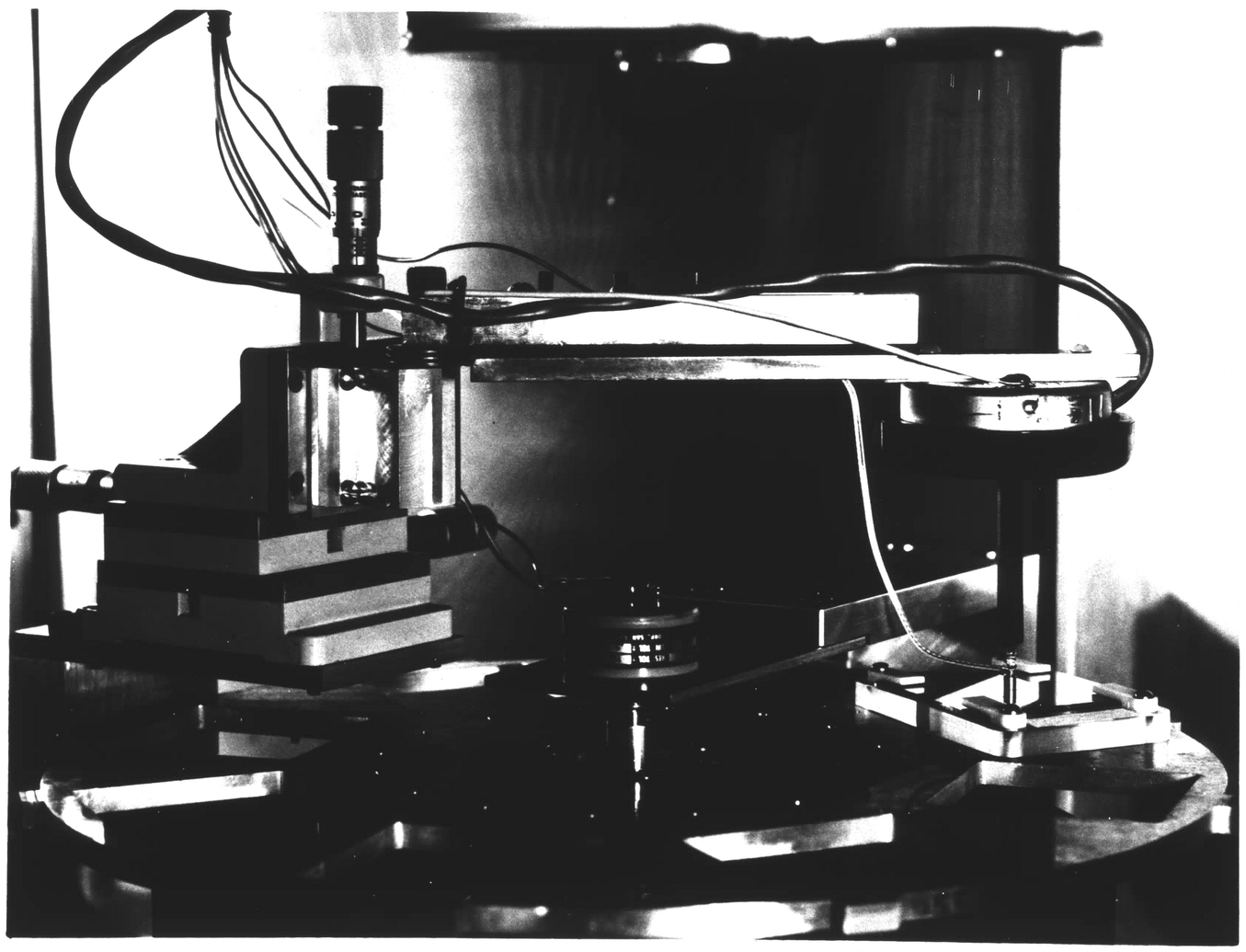

FIGURE 6

PHOTOGRAPH OF EQUIPMENT.
ELECTRON BEAM AND VACUUM CHAMBER ARE
LOCATED IN CENTER. BEAM OPERATING
APPARATUS IS ON RIGHT AND KELVIN
PROBE OPERATING EQUIPMENT ON LEFT

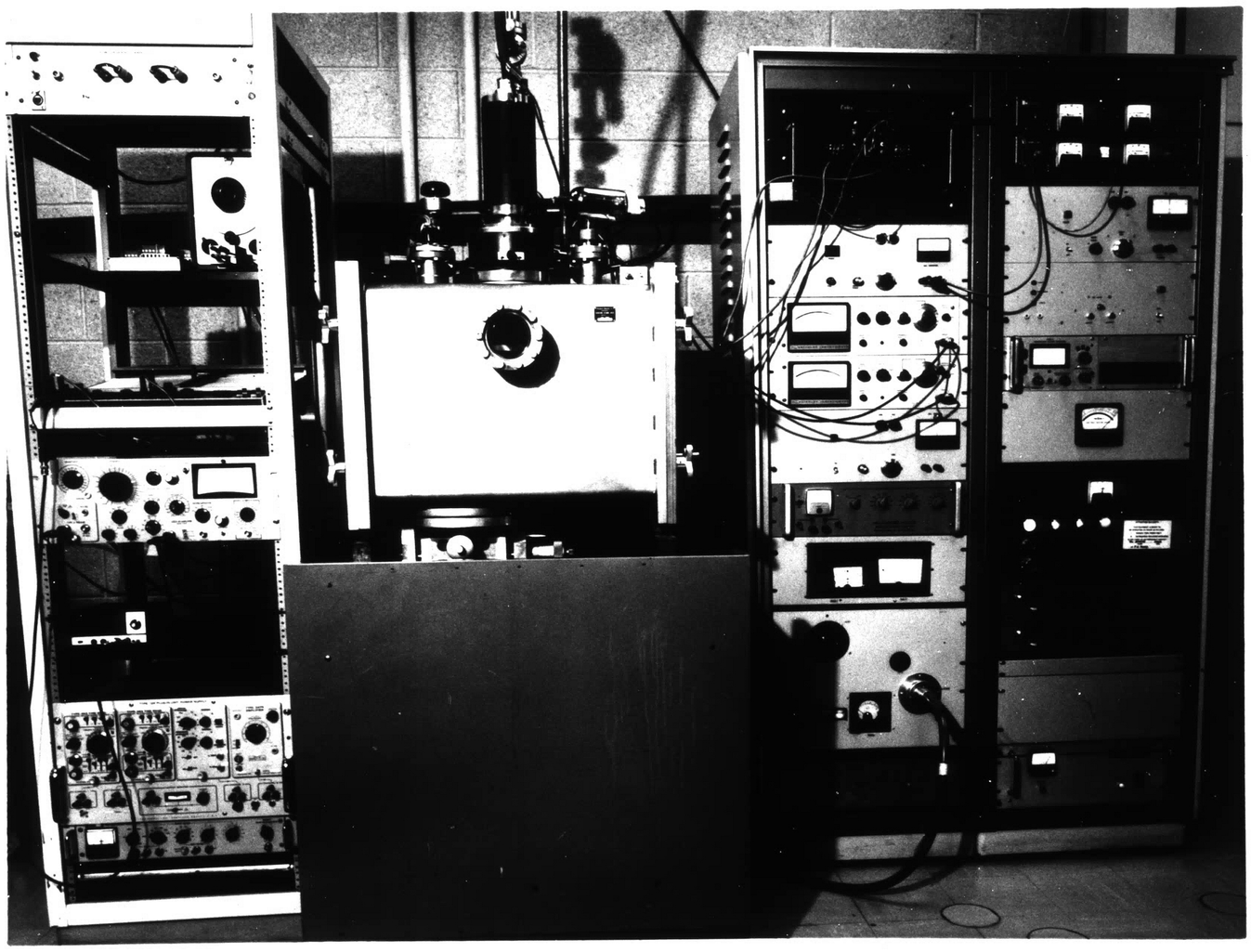

FIGURE 8

FROM LEFT TO RIGHT: SAMPLE IN SAMPLE HOLDER, FARADAY CUP, COPPER PLATE FOR BEAM SIZE DETERMINATION APPROX. 1/4 FULL SIZE

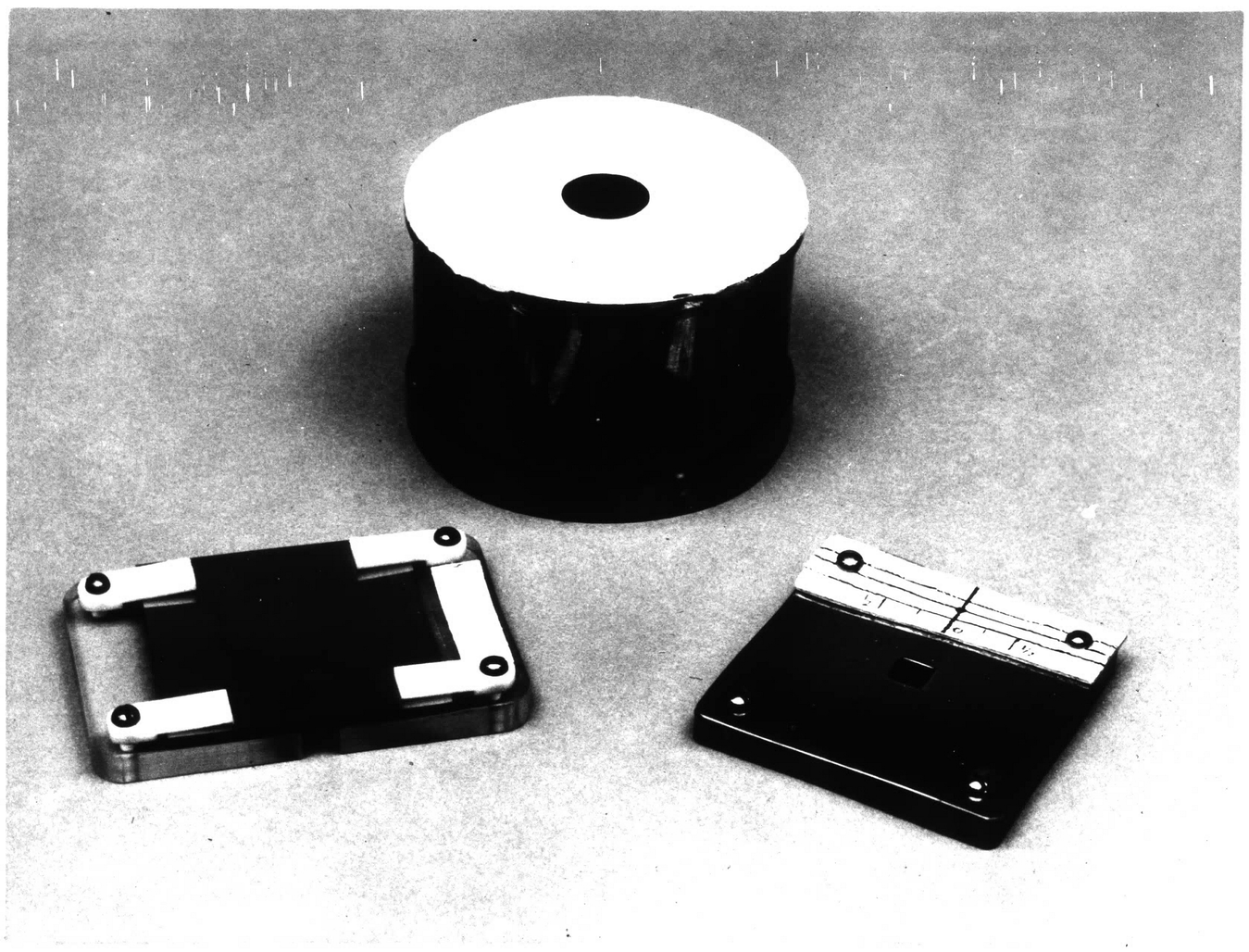

FIGURE 9
CURRENT PATTERN GENERATED
DURING BEAM SIZE DETERMINATION

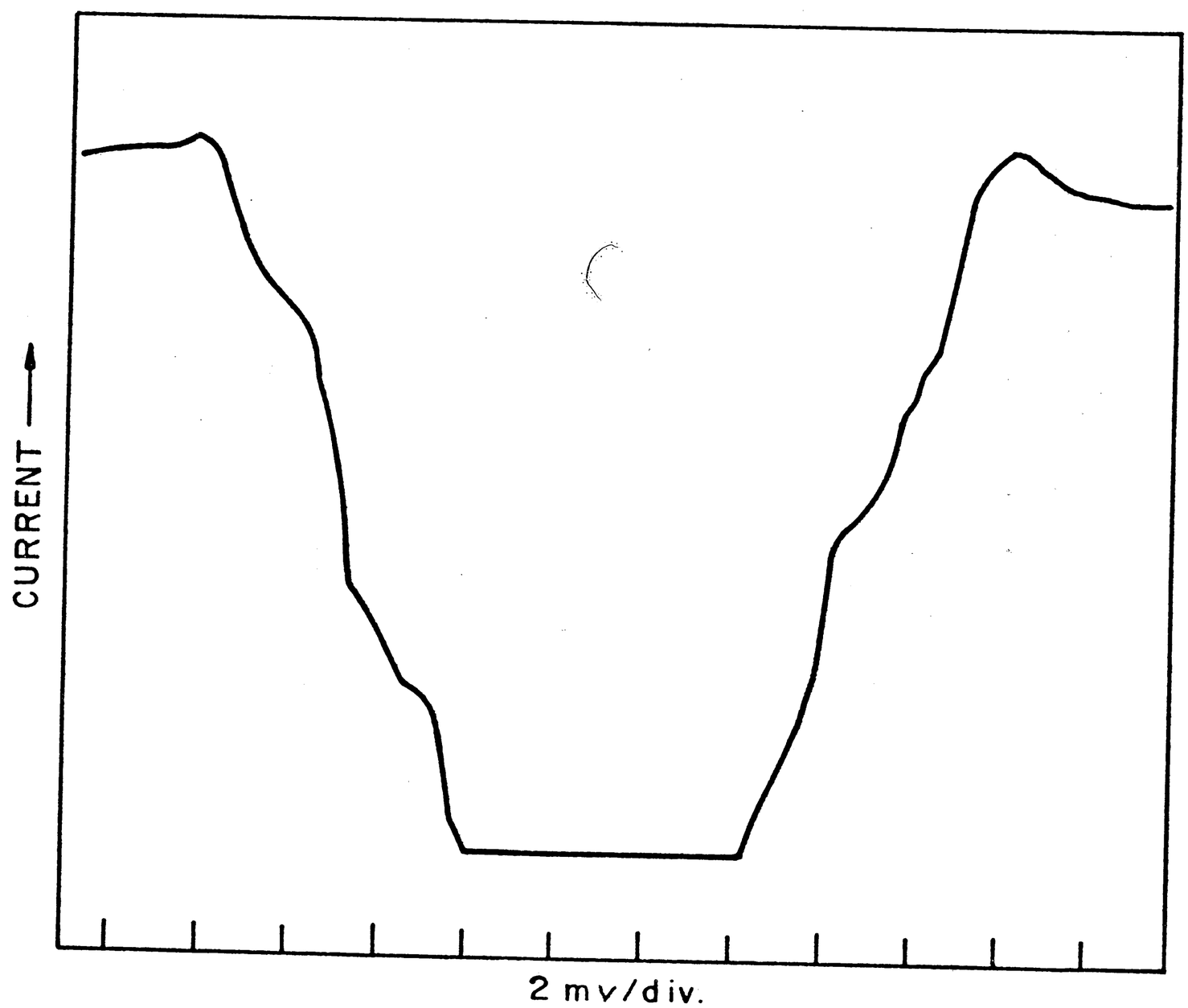

FIGURE 10

TYPICAL CHARGE PROFILES ON DIFFERENT TYPES OF MATERIALS

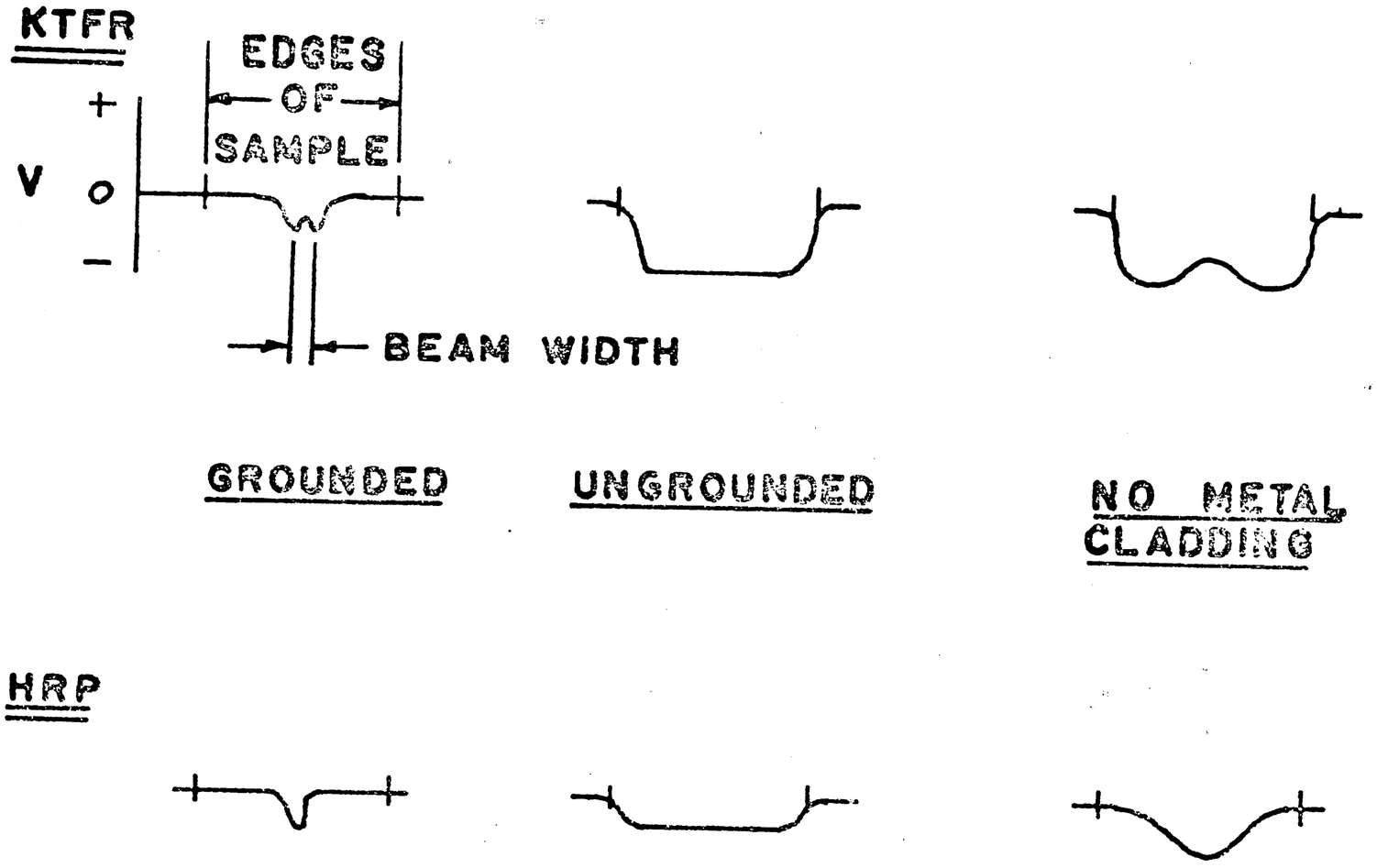

FIGURE 11

DECAY OF SURFACE POTENTIAL ON METAL CLAD KTFR. 6.2×10^{-5} COUL/CM^2 - X, 6.2×10^{-1} COUL/CM^2 - O 6.2×10^{-7} COUL/CM^2 - ●. ALL AT 15 KV. UPPER THREE CURVES ARE UNGROUNDED, LOWER THREE ARE GROUNDED

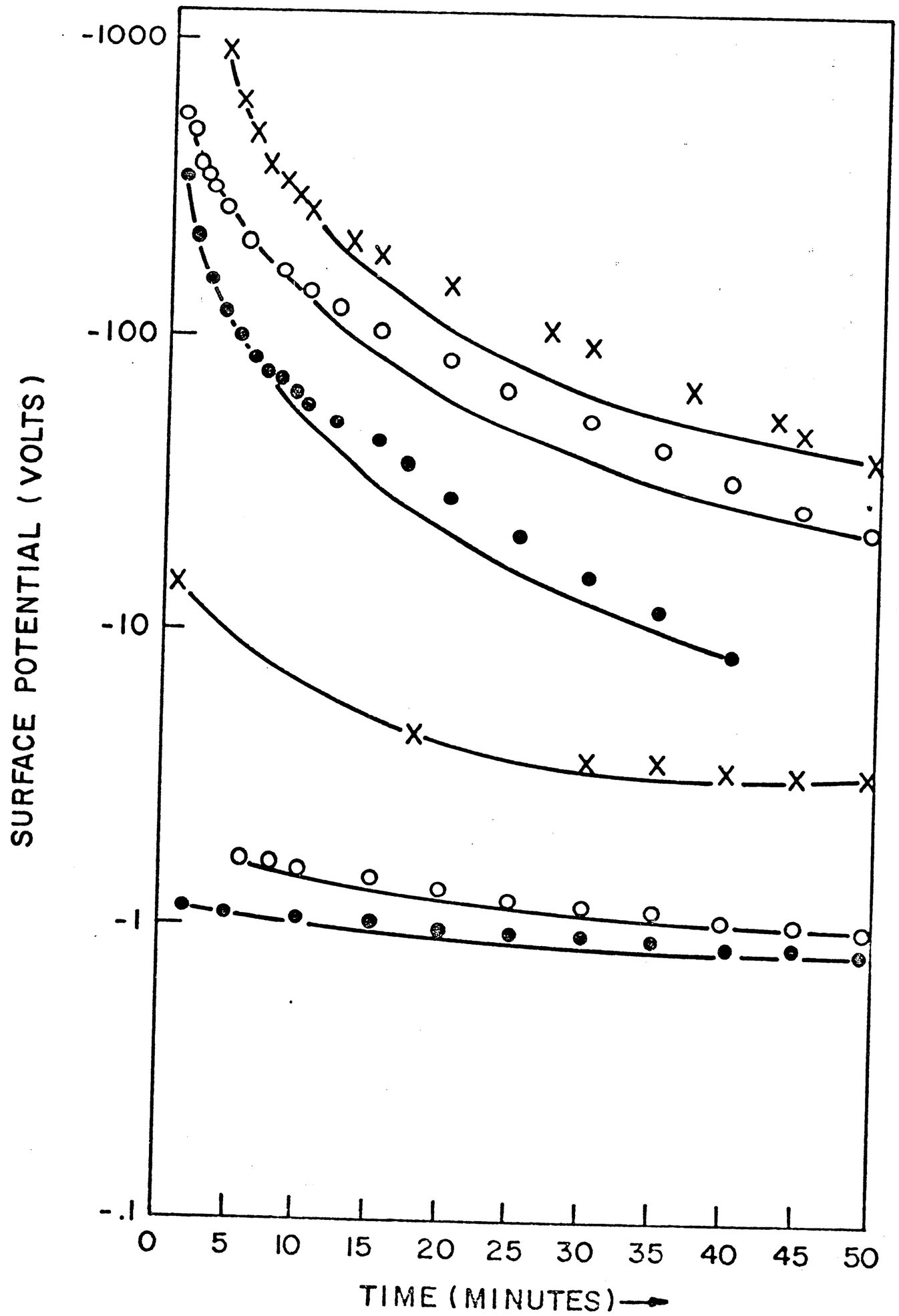

FIGURE 12

DECAY OF SURFACE POTENTIAL ON METAL CLAD HRP. 6.2×10^{-8} COUL/CM^2 - X, 6.2×10^{-9} COUL/CM^2 - O 6.2×10^{-10} COUL/CM^2 - ●. ALL AT 15 KV. UPPER THREE CURVES ARE UNGROUNDED, LOWER THREE ARE GROUNDED.

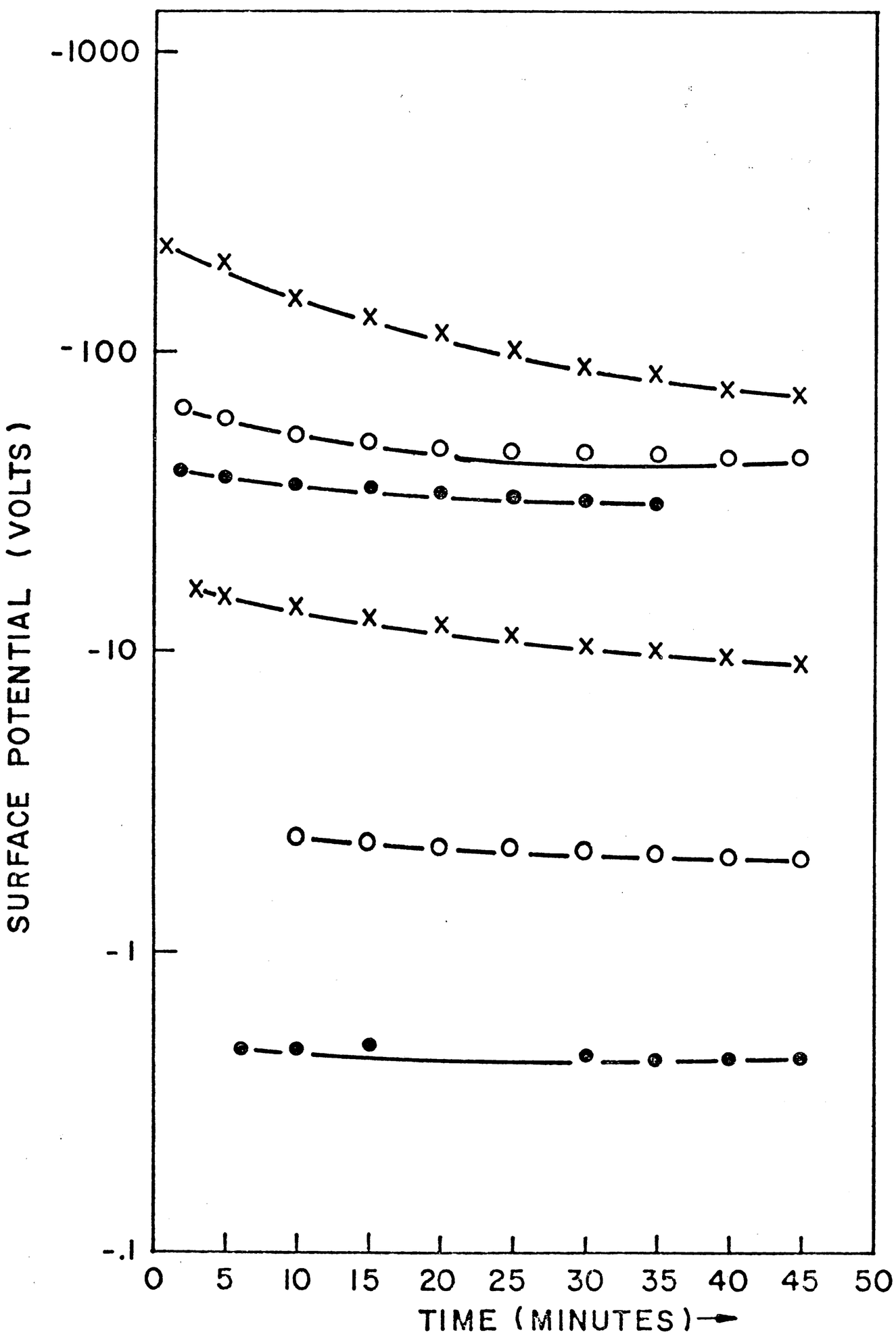

FIGURE 13
DECAY OF SURFACE POTENTIAL ON
METAL CLAD UNGROUNDED KTFR. 15 KV-X, 10 KV -O
5 KV-●. ALL AT DOSE OF 6.2×10^{-6} COUL/CM^2

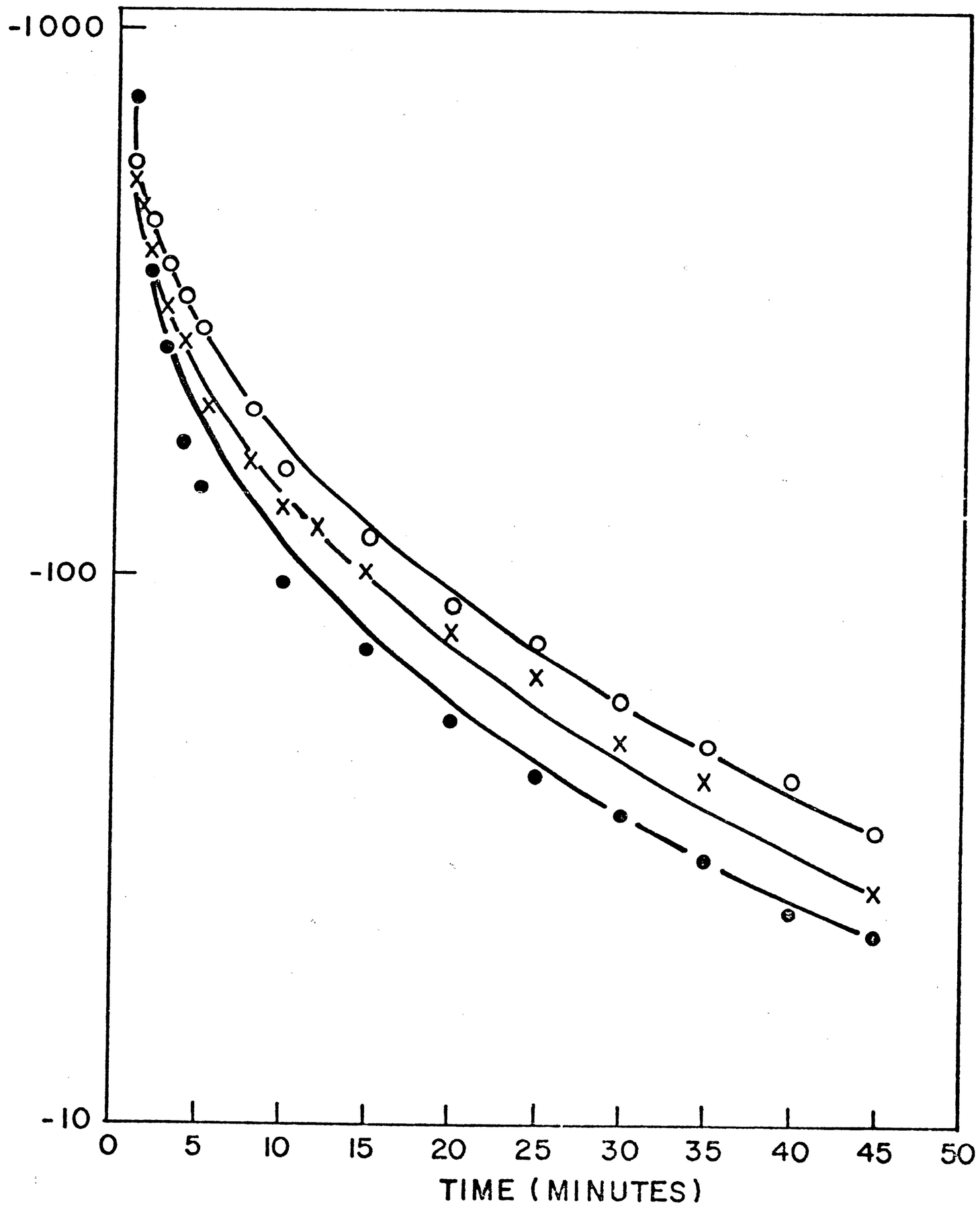

FIGURE 14
DECAY OF SURFACE POTENTIAL ON
METAL CLAD GROUNDED HRP. 15KV-X, 10KV-O
5KV-● ALL AT DOSE OF 6.2×10^{-9} COUL/CM^2

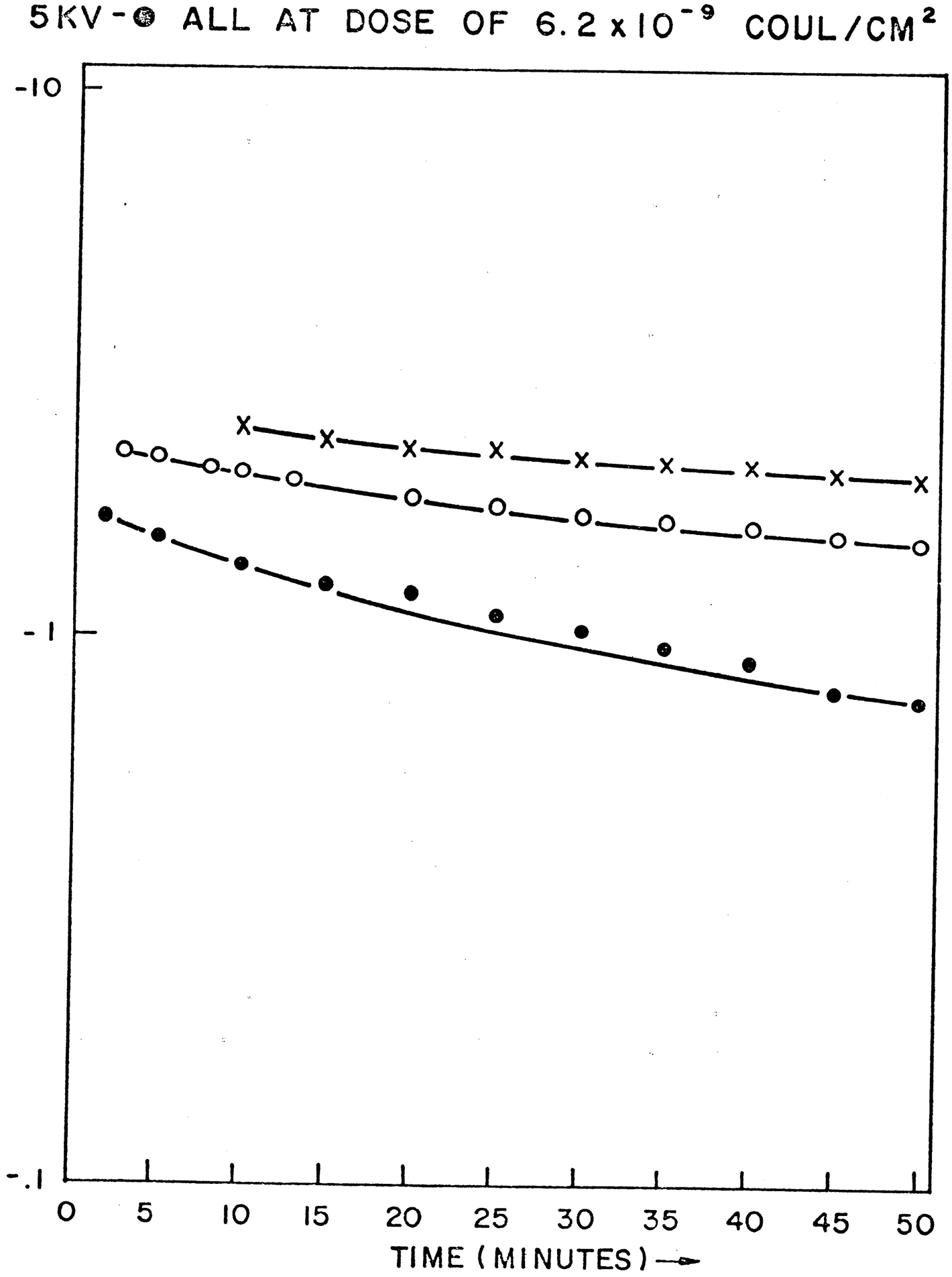

FIGURE 15

DECAY OF SURFACE POTENTIAL ON METAL CLAD GROUNDED KTFR. 15 KV–X, 10 KV-O 5KV-●. ALL AT DOSE OF 6.2×10^{-7} coul/cm^2

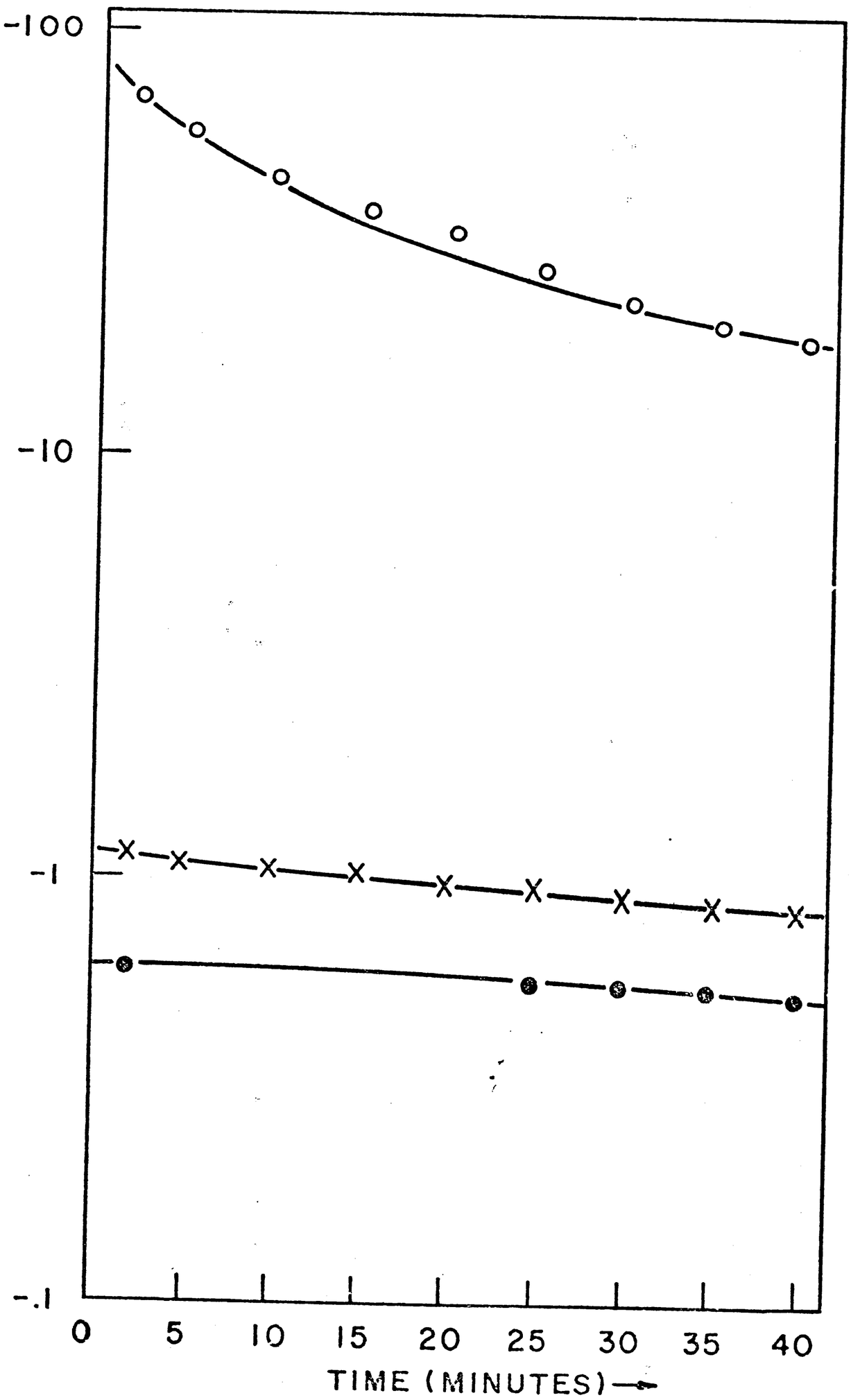

FIGURE 16

CHARGE REDISTRIBUTION ON KTFR.

DOSE IS 6.2×10^{-5} coul/cm^2 AT 10 KV

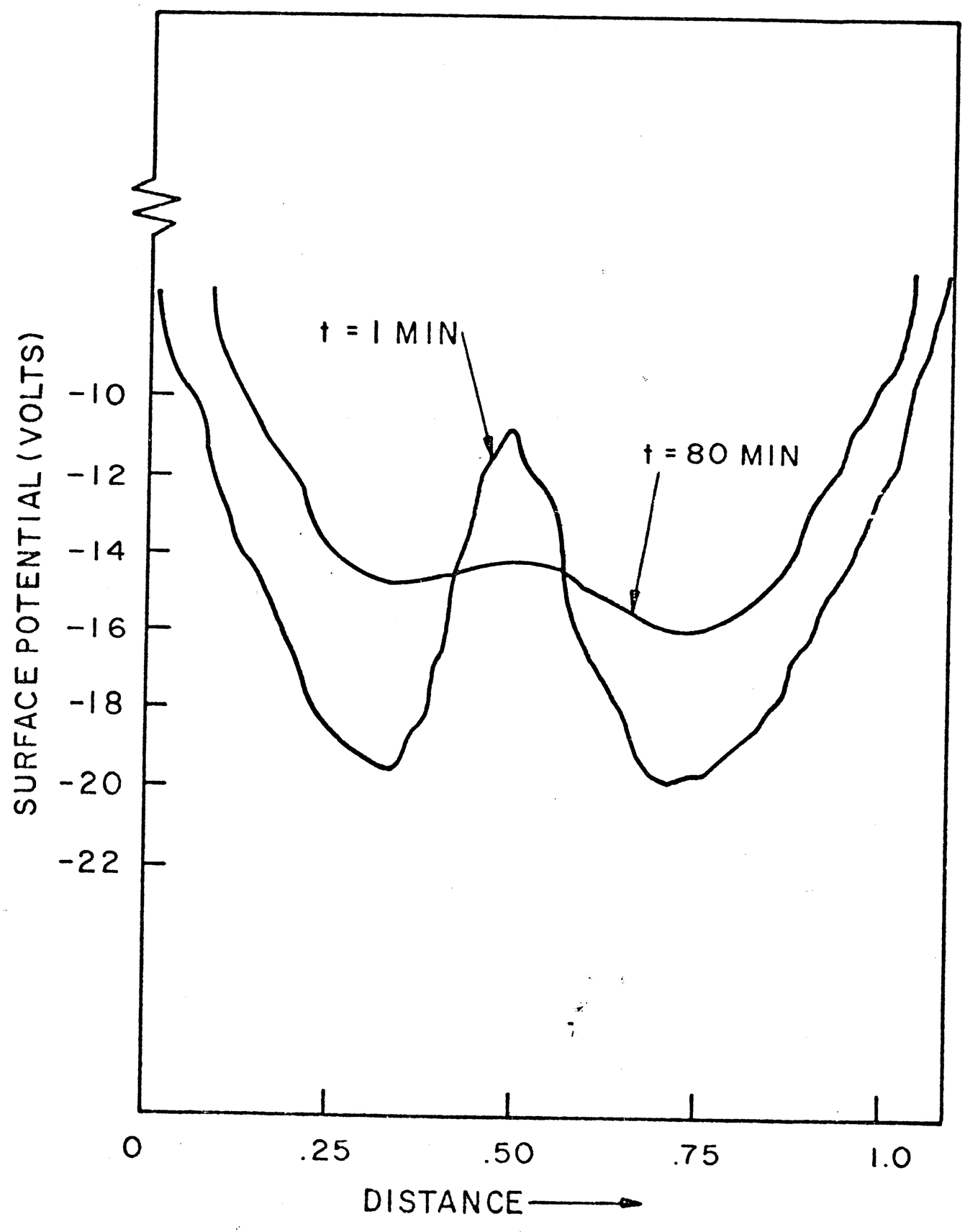

FIGURE 17

DECAY OF SURFACE POTENTIAL ON METAL CLAD GROUNDED KTFR MEASURED ON POSITIVE PEAK. 15 KV AND 6.2×10^{-7} coul/cm^2 DOSE

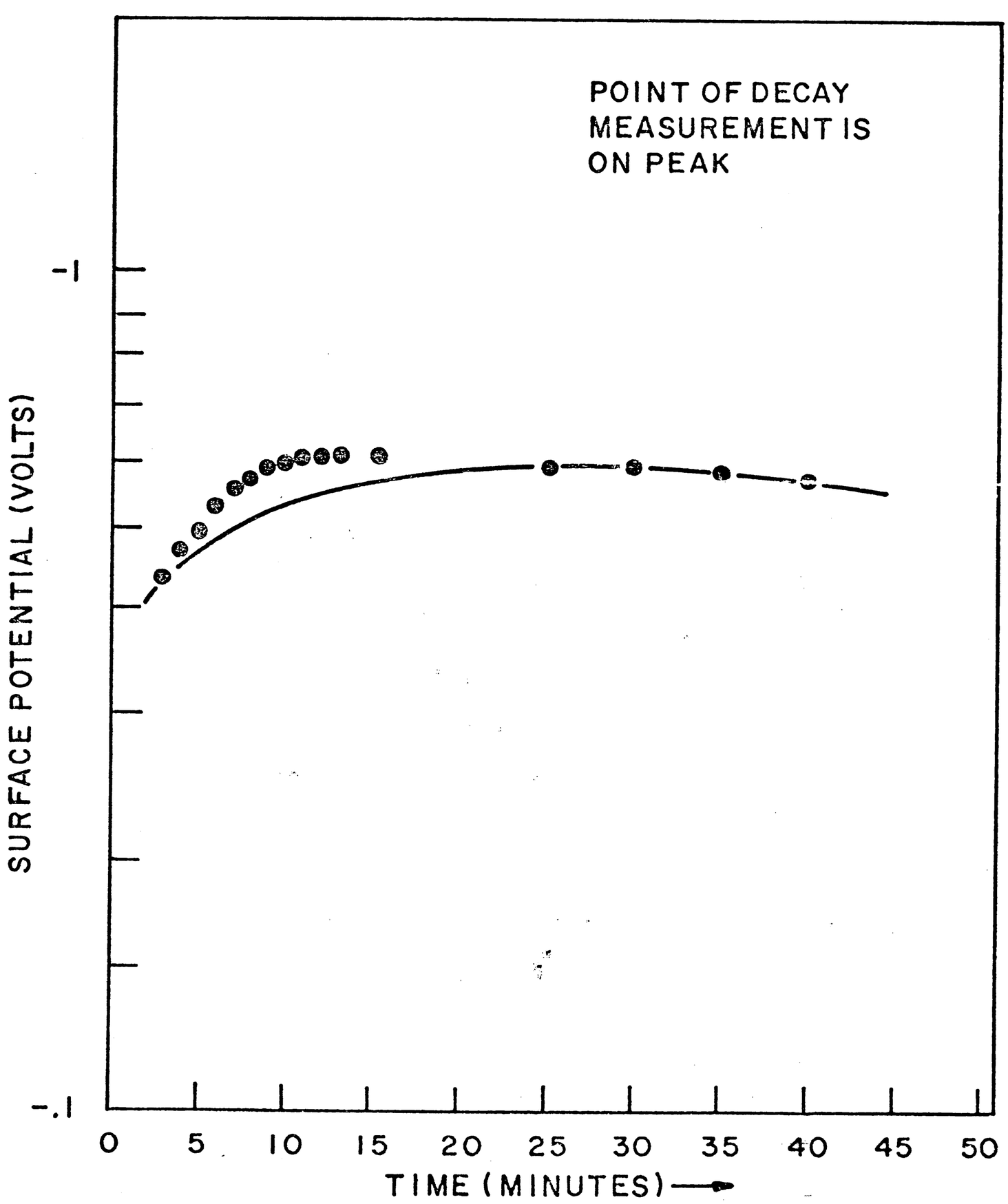

FIGURE 18

EFFECTS OF ATMOSPHERE PRESSURE ON CHARGE STORED ON KTFR; METAL CLAD, GROUNDED. DOSE IS 6.2×10^{-6} COUL/cm^2 AT 10 KV

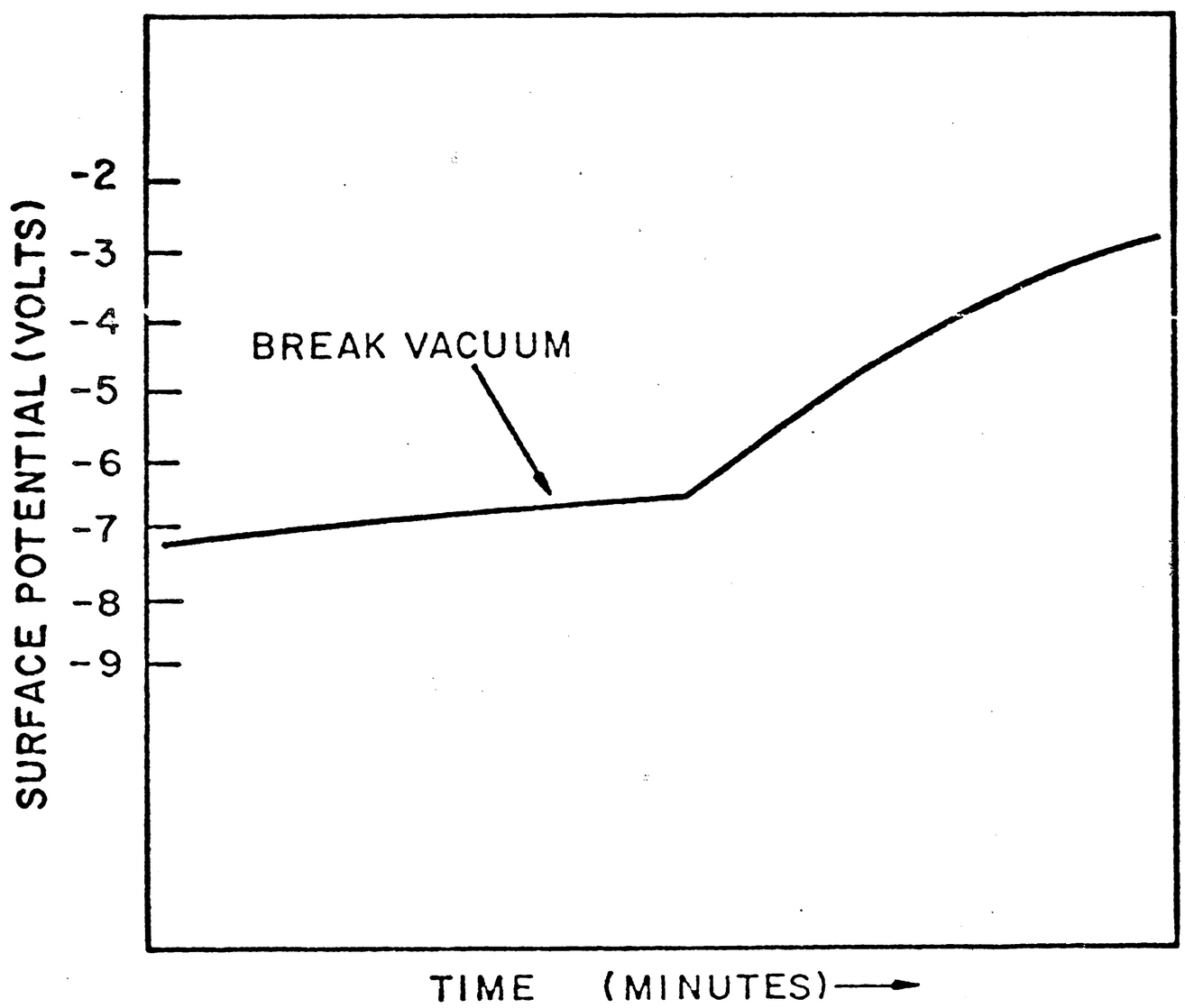

FIGURE 19
SLOW DECAY OF CHARGE ON SILICON WAFER

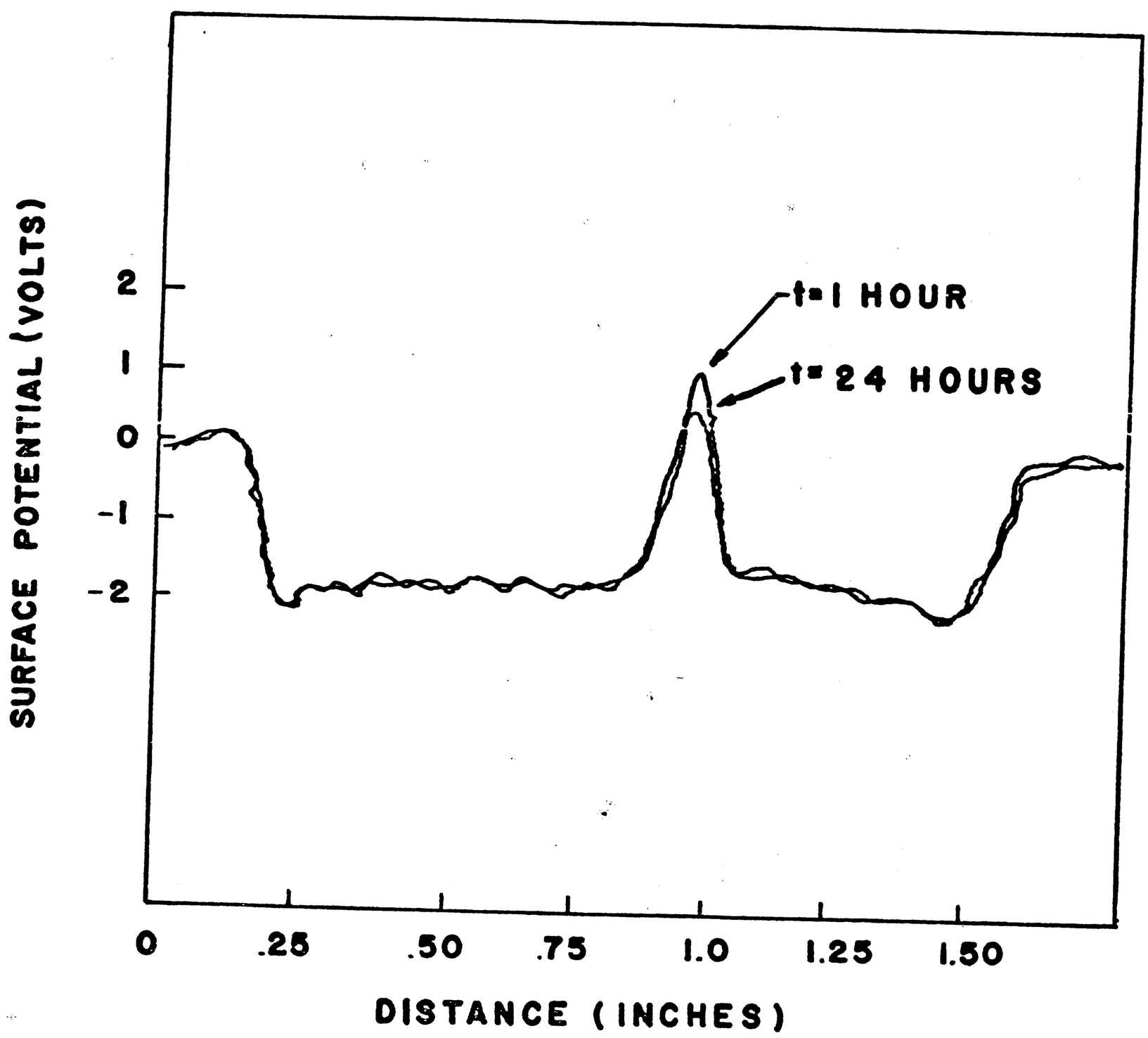

FIGURE 20

CHARGE PROFILE ON SILICON WAFER BEFORE AND AFTER KTFR REMOVAL

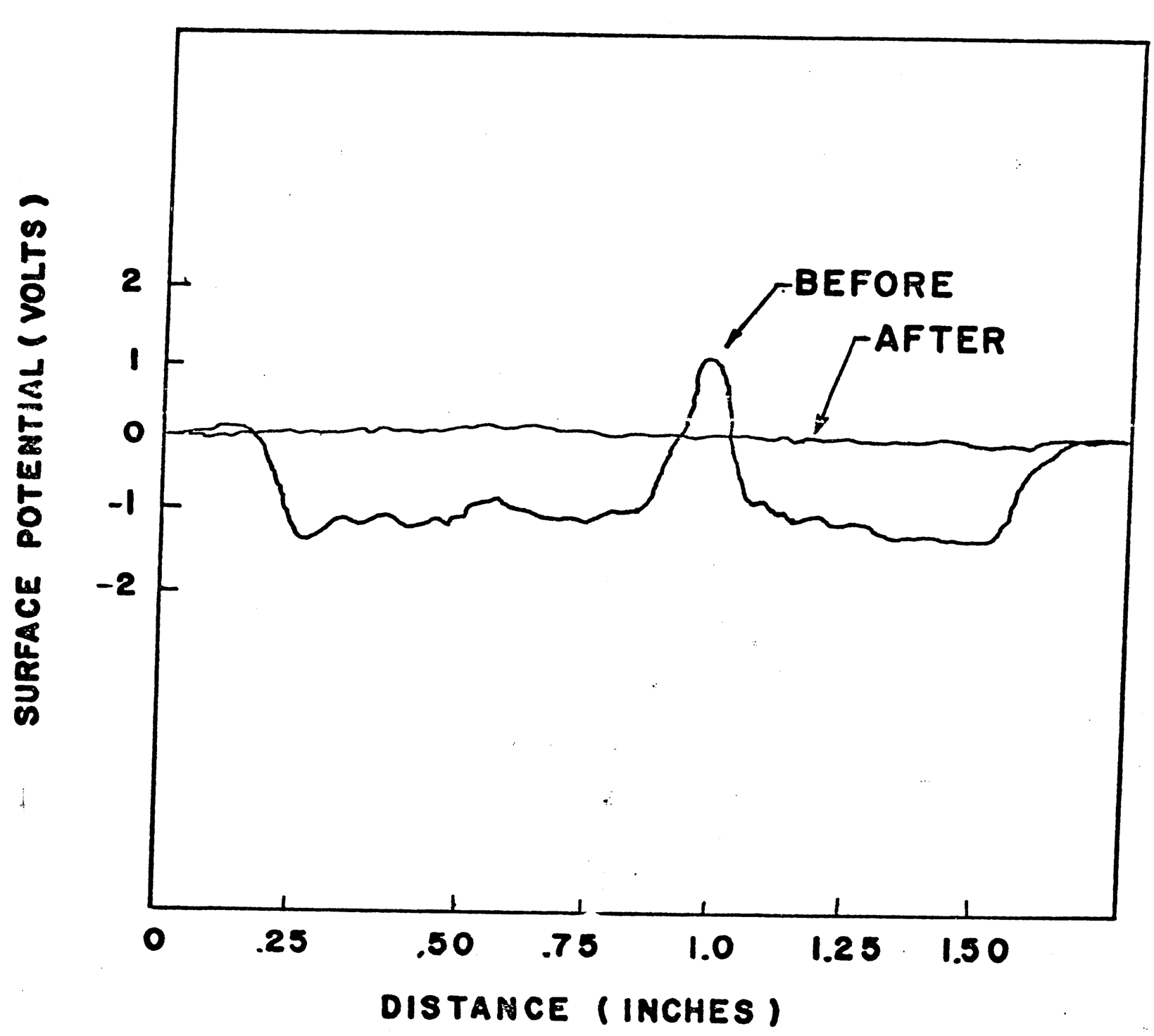

FIGURE 21

COMPARISON OF RATES OF DOSE

TOTAL DOSE IS 6.2×10^{-6} coul/cm^2 AT 15 KV

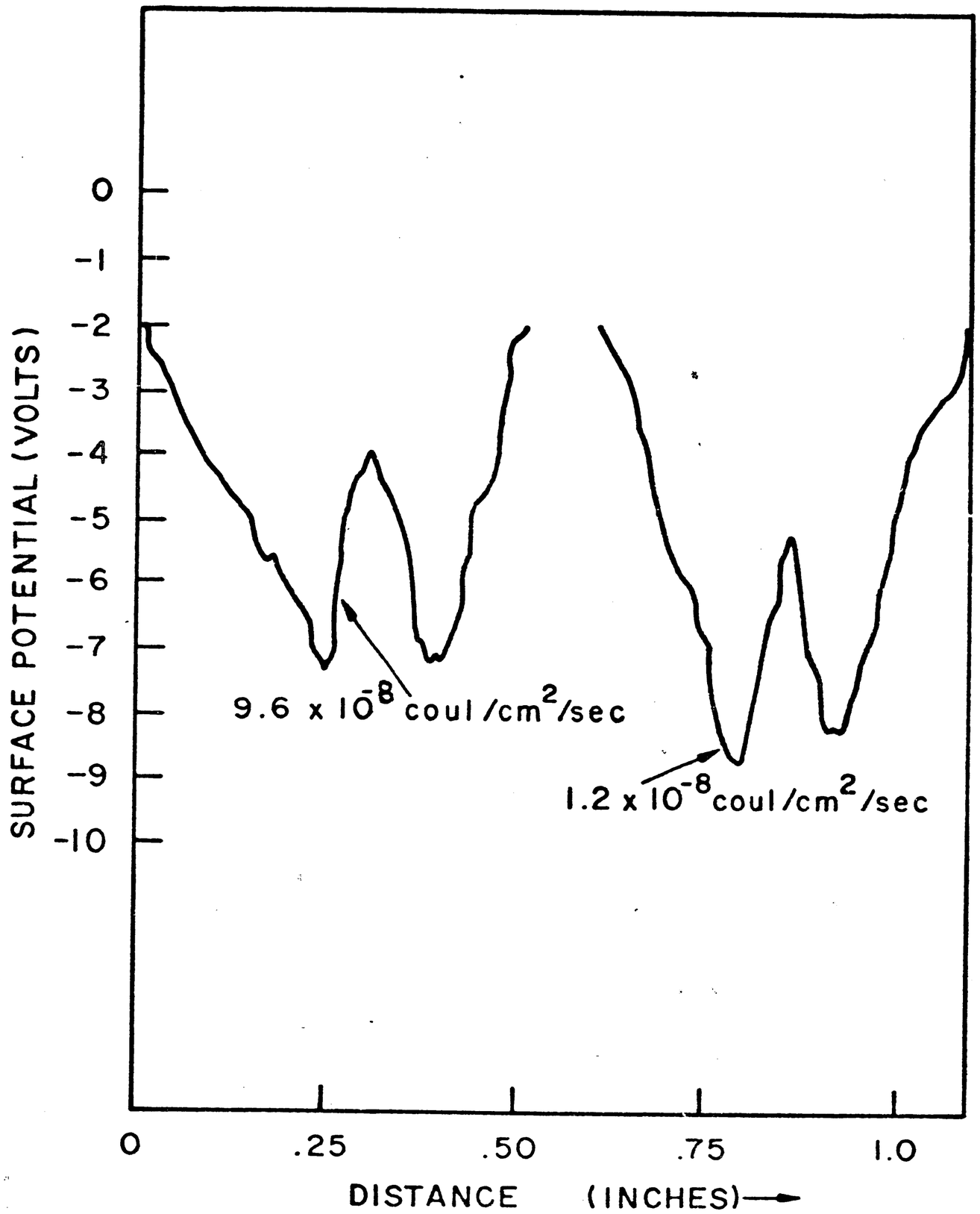

FIGURE 22

DECAY OF SURFACE POTENTIAL ON KTFR WITH NO METAL CLADDING. 6.2×10^{-5} COUL/CM^2 - X 6.2×10^{-6} COUL/CM^2 - O, 6.2×10^{-7} COUL/CM^2 ●. ALL AT 15 KV

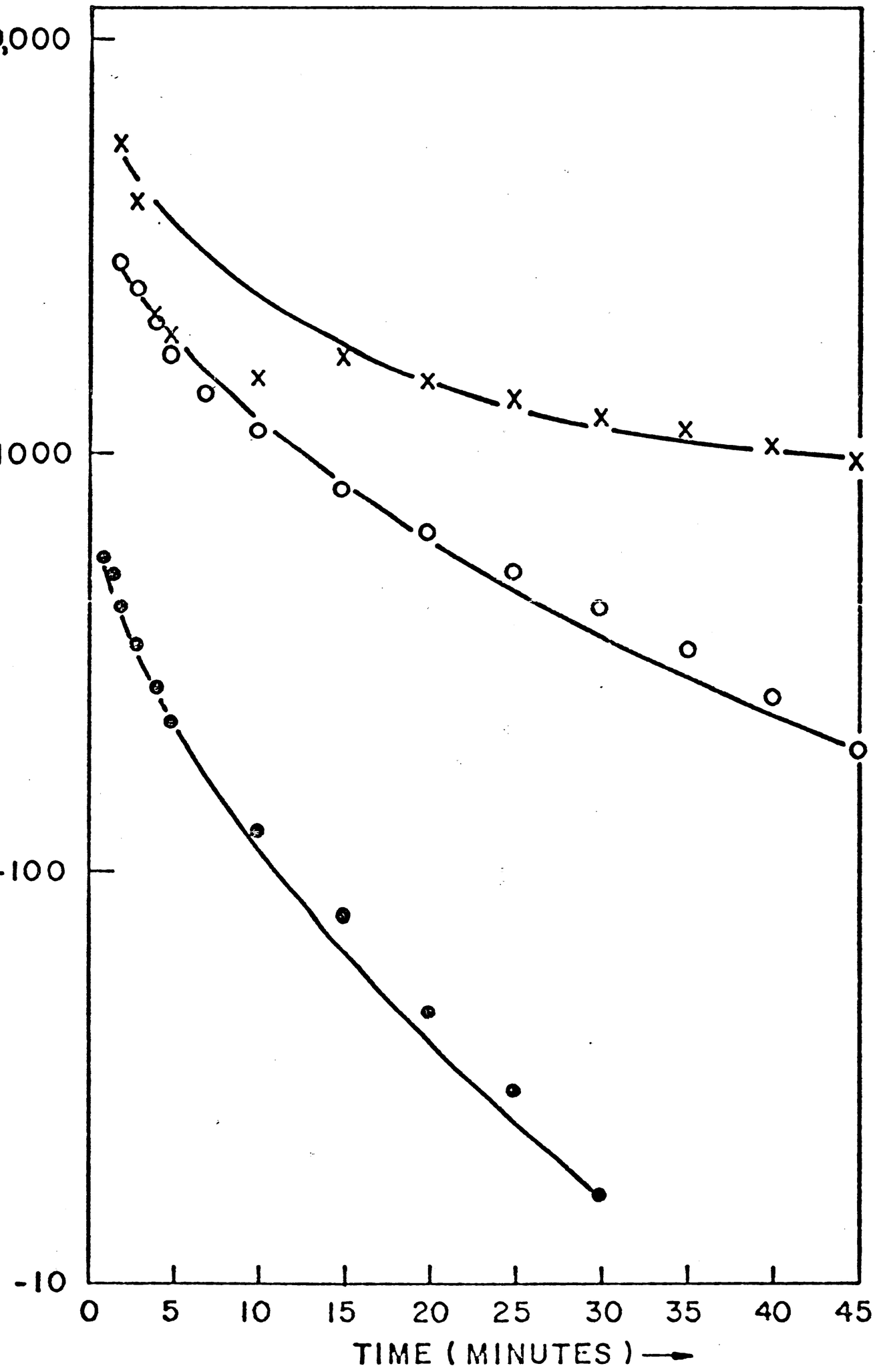

FIGURE 23

DECAY OF SURFACE POTENTIAL ON
HRP WITH NO METAL CLADDING.
6.2×10^{-7} coul/cm^2 -X 6.2×10^{-8} coul/cm^2 -O,
6.2×10^{-10} coul/cm^2 -O. ALL AT 15 KV.

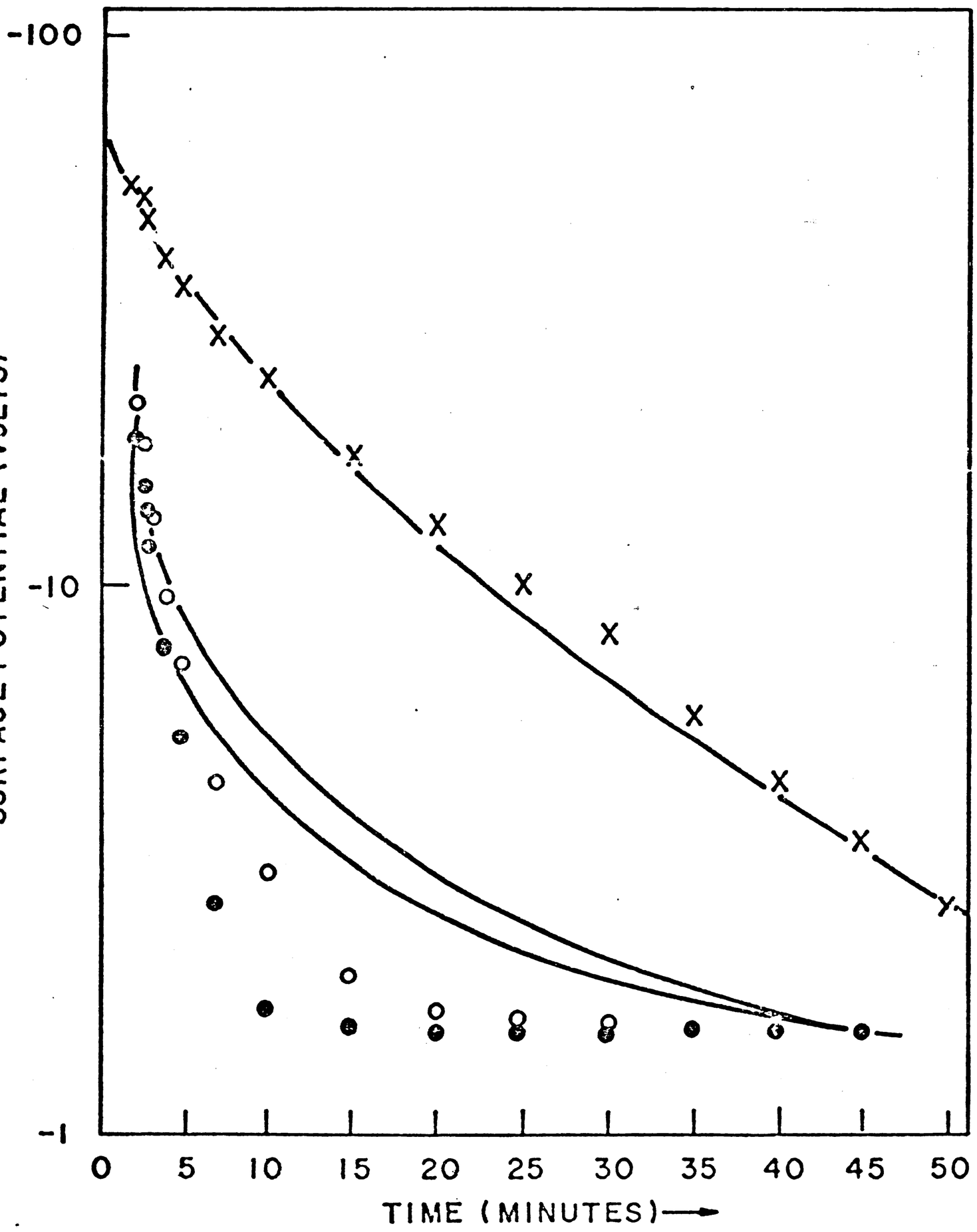

BIBLIOGRAPHY

1. Stern, Lothar, Fundamentals of Integrated Circuits, Motorola, 1968.

2. Howland, F. L., and Poole, K. M., pp. 1997 to 2009, Bell System Technical Journal, November, 1970.

3. Thornley, R. F. M., and T. Sun, Journal of the Electrochemical Society, 1965.

4. Perkins, K. D., and R. Bennett, Kodak Photoresist Seminar Proceedings, 1968 Edition, Volume II, pp. 39-46.

5. Samaroo, W. R., B. Broyde, and M. W. Sagal, Western Electric Company, private communication, with permission.

6. James, T. H., editor, The Theory of the Photographic Process, third edition, The Macmillan Company, New York, 1966.

7. Kornfeld, W., Photoresist Technology Improvement, Part I, Motorola.

8. Charlesby, A., Atomic Radiation and Polymers, Pergamon Press, 1960.

9. Broyde, B., Western Electric Company, private communication,with permission.

10. Shaw, E., Physics Review, 44, 1933, 1009.

11. Stewart, R. L., Physics Review, 45, 1935, 488.

12. Aston, F. W., Mass Spectra and Isotopes, Longman, Green and Co., New York, 1942.

13. Lindholm, E., Review of Scientific Instruments, 31, 1960, 210.

14. Munakata, Kohno, Maekawa, Honda and Miura, Japan J. Appl. Phys. 9 (1970), 1187-1188.

15. Stern, H. A., Proceedings of Kodak Photoresist Seminar, May 19-20, 1969.

16. Zisman, W. A., Review of Scientific Instruments, Vol. 3, 1932, 367-370.

BIBLIOGRAPHY (Cont'd)

17. Parker, J. H., and R. W. Warren, The Review of Scientific Instruments, Vol. 33, No. 9, 1962.

18. Pettit-Clerc, Y., and J. D. Carette, The Review of Scientific Instruments, 1968.

19. Craig, P. P. and Radeka, V., Review of Scientific Instruments, Vol. 41, No. 2, 1970.

20. Rodriguez, F., Principles of Polymer Systems, McGraw-Hill, Inc., 1970, pg. 272.

VITA

Arthur K. Kreider was born on June 19, 1935, in Lebanon, Pennsylvania. He attended Public Schools in Lebanon County, graduating from Lebanon High School in 1953.

After attending the Penn State Center in York, Pennsylvania, from 1954 to 1956 he received an Associate's Degree in Electrical Engineering.

He was employed by Western Electric in June of 1956 as an Engineering Associate. In 1965 he was promoted to planning engineer. After attending evening school from 1959, he received a Bachelor's Degree in Electrical Engineering from Villanova University in June of 1969.

In 1969 he entered the Graduate School of Lehigh University as a member of Western Electric's Lehigh Master's Program.